Hydration Energies of Iron Hydroxide Cation: A Guided Ion Beam and Theoretical Investigation

Oxana Sander[†] *and P. B. Armentrout*[‡,]*

[†] Fachbereich Chemie, Technische Universität Darmstadt, Alarich-Weiss-Str.8, 64287 Darmstadt, Germany.

[‡] Department of Chemistry, University of Utah, 315 S. 1400 E. Rm 2020, Salt Lake City, Utah 84112, USA.

ABSTRACT: We present experimental collision-induced dissociation (CID) cross sections as a function of kinetic energy for $FeOH^+(H_2O)_n$, where n = 1 – 4, with xenon (Xe) obtained using a guided ion beam tandem mass spectrometer. Complexes with n = 2 – 4 are observed to undergo water loss, followed by sequential water loss at higher collision energies. In addition, we find that loss of the neutral hydroxide group is competitive with the primary water loss for n = 1. Bond dissociation energies (BDEs) at 0 K are derived through modeling the experimental cross sections after accounting for multiple collisions, kinetic shifts, and reactant internal and kinetic energy distributions. Quantum chemical calculations include geometry optimizations performed at a B3LYP/6-311+G(d,p) level of theory and then used for single point calculations at B3LYP, B3P86, MP2, and CCSD(T) levels with a 6-311+G(2d,2p) basis set. Additional geometry optimizations at the cam-B3LYP/def2-TZVP were also performed as well as empirical dispersion corrections at all levels. The various structures for the $FeOH^+(H_2O)_n$ complexes and their relative energies are discussed in detail. We also derive experimental BDEs for the OH-loss from $FeOH^+(H_2O)_n$, with n = 2 – 4, using the experimental BDE of n = 1 in combination with literature data for water loss from $Fe^+(H_2O)_n$ species. Measurements of BDEs for hydroxide and water loss from $FeOH^+(H_2O)_n$ (n = 1 – 4) are the first such experimental measurements. Theoretically calculated BDEs are in reasonable agreement for water loss from both $FeOH^+(H_2O)_n$ and $Fe^+(H_2O)_n$ complexes and for $D_0(Fe^+\text{-}OH)$, but are too low for the loss of OH from the larger hydrated complexes.

INTRODUCTION

Iron is the fourth most abundant element in the earth's crust and is usually found in the form of oxides, sulfides, or carbonates.[1] It is an essential trace element necessary to many living organisms where it is responsible for oxygen transport through hemoglobin and electron transport in photosynthetic and respiratory systems through cytochrome c.[2] The metal ion containing active site of a protein is very sensitive to its surroundings.[3] Water is the major solvent in the biochemical environment of proteins as well as in many chemical reactions catalyzed by transition metal complexes. It is therefore of great interest to understand the basic interactions of water molecules with metal ions. This knowledge can then be extended and refined to include other ligands for a more sophisticated discussion of reaction mechanisms as they occur in real systems.

While solvated bivalent iron and gas-phase hydrated bivalent iron complexes have been well studied,[4-8] less is known about hydrated iron hydroxides. Recently, $FeOH^+(H_2O)_n$ complexes with n = 1 – 4 were studied by Garand and co-workers using infrared vibrational predissociation spectroscopy,[9] providing structural information for these species. Hydrated metal hydroxide cations also appear as fragments of $M^{2+}(H_2O)_n$ complexes that undergo a proton transfer according to the charge separation reaction 1.

$$M^{2+}(H_2O)_n \rightarrow MOH^+(H_2O)_{n-m-1} + H^+(H_2O)_m \quad (1)$$

Kebarle and co-workers[10] showed that this reaction occurs when the number of water molecules is lower than a critical number n_{crit}. For M = Fe, these authors suggested n_{crit} to be between 4 and 5, whereas Shvartzburg and Siu later indicated $n_{crit} = 5$.[11] This value corresponds well with the smallest $Fe^{2+}(H_2O)_n$ complex that could be generated directly from solution using an electrospray ionization source under atmospheric conditions and analyzed through guided ion beam techniques in our group.[12] However, analysis of the experimental collision-induced dissociation (CID) cross sections in this work assigned n_{crit} as 4 using an energy-dependent definition of critical size.[13] Hydration energies of $Fe^{2+}(H_2O)_n$ complexes were reported over a size range of 4 to 11.[12] An interesting question is how binding energies change when one water is replaced by a hydroxide group. Thus, the present study aims to determine sequential bond dissociation energies (BDEs) for

water loss from $FeOH^+(H_2O)_n$ clusters with n = 1 – 4 using a guided ion beam tandem mass spectrometer (GIBMS). These results are combined with results of quantum chemical calculations to discuss the trends in the hydration energies of iron and iron hydroxide cations. It also contributes to furthering our systematic study of transition metal hydroxide hydration energies that also includes work on $CuOH^+(H_2O)_n$ and $CoOH^+(H_2O)_n$ complexes.[14,15]

As will be seen below, the main dissociation pathways of $FeOH^+(H_2O)_n$ are the loss of a neutral water molecule in reaction 2, but the loss of the neutral hydroxide radical in reaction 3 is also observed uniquely for dissociation of the $FeOH^+(H_2O)$ complex.

$$FeOH^+(H_2O)_n \rightarrow FeOH^+(H_2O)_{n-1} + H_2O \quad (2)$$

$$FeOH^+(H_2O) \rightarrow Fe^+(H_2O) + OH \quad (3)$$

The former reaction can be followed by sequential water losses when the available energy is high enough and n ≥ 2. In their study of $FeOH^+(H_2O)_n$ complexes with n = 1 – 4, Garand and co-workers[9] considered at least two isomers for the $FeOH^+(H_2O)_4$ complex in order to explain their experimental results. Because they thermalized their complexes at 10 K, more isomers might be accessible under the room temperature conditions utilized in the present work, even for smaller complexes, and will thus be considered in the present work. Although theoretical hydration energies of $FeOH^+(H_2O)_n$ complexes have been reported by Garand et al., we present experimental BDEs of the primary and secondary water loss from $FeOH^+(H_2O)_n$ with n = 1 – 4 for the first time as measured using a GIBMS. The experimental BDEs are then used to evaluate different theoretical methods regarding their accuracy to predict those energies. Finally, the $FeOH^+$ hydration energies are combined with experimental results from Dalleska et al.[8] of the BDEs for water loss from $Fe^+(H_2O)_n$ complexes, which also enables us to report experimental BDEs for OH radical loss from $FeOH^+(H_2O)_n$ with n = 1 – 4.

EXPERIMENTAL and COMPUTATIONAL METHODS

Experimental approach

The Utah GIBMS has been described in detail previously.[16,17] Here, $FeOH^+(H_2O)_n$ ions were produced using an electrospray ionization (ESI) source[18] from a 10^{-4} M water solution of $FeSO_4$. A voltage of about 2.3 kV was applied to the ESI needle and sample was introduced at a rate of 0.035 ml/h into the first vacuum stage using a heated capillary (80 °C). Once in the gas phase, ions were confined and focused by a radio frequency (rf) ion funnel using a dc gradient drift field and transferred into a rf hexapole ion guide. Ions were thermalized while drifting through the hexapole by undergoing more than 10^4 collisions with ambient gas. To improve signal intensity of desired $FeOH^+(H_2O)_n$ species, an in-source fragmentation technique of larger complexes was applied using electrodes in the hexapole region.[19] It has been shown previously that ions produced through this in-source fragmentation method undergo enough collisions to be thermalized under appropriate experimental conditions.[19-21]

Ions were then extracted into the next vacuum stage and focused before being introduced into a magnetic sector field analyzer where the desired reactant ions were mass selected. These were subsequently focused and decelerated to a known kinetic energy, E_{Lab}, before being injected into a rf octopole ion guide.[16,22] The kinetic energies of the ions were varied by floating the ion guide to a desired potential. Retarding potential techniques were used to determine the absolute zero of kinetic energy and the ion kinetic energy distribution.[16] On their way through the octopole, ions pass through a collision cell where xenon (Xe*)* gas was introduced to induce ion fragmentation. Typical gas pressures for dominantly single collision conditions lie between 0.05 – 0.2 mTorr. As the collision cell enclosed the octopole rods, reactant as well as product ions were trapped and passed into the last focusing stage before mass analysis with a quadrupole mass filter and detection using a Daly detector.[23]

Data Analysis

Measured ion intensities were converted to reaction cross sections using a Lambert-Beer-like approach described previously.[16] The lab-frame collision energy E_{Lab} is transformed to the center-of-mass frame (CM) collision energy using $E_{CM} = E_{Lab} \times m / (m + M)$, with m being the

mass of the collision gas Xe and *M* the reactant ion mass. All energies discussed below are in the CM frame. The retarding potential technique yields a kinetic energy distribution with a full width at half-maximum of 0.15 – 0.20 eV. To obtain accurate thermochemical results from the data analysis, single collision conditions are crucial. Even when the collision gas pressure is chosen such that the mean free path exceeds the cell length by several orders of magnitude, a probability for secondary collisions still remains. Therefore, reaction cross sections were determined at three different gas pressures in the low-pressure region (~0.05, 0.1, and 0.2 mTorr) and extrapolated to zero pressure. Collisions occurring outside the collision cell were accounted for by measuring product intensities without collision gas in the gas cell and subtracting this from the intensity measured with collision gas in the gas cell.

To determine bond dissociation energies, reaction cross sections were modeled using the following empirical equation:

$$\sigma_j(E) = \sigma_{0,j} \sum_i g_i \, (E + E_i - E_{0,j})^N / E \qquad (4)$$

Here, $\sigma_j(E)$ is the reaction cross section for reaction channel *j* with a corresponding 0 K reaction threshold $E_{0,j}$, $\sigma_{0,j}$ is an energy independent scaling factor, *E* is the relative collision energy of the collision partners, *N* is a parameter describing the efficiency of energy transfer,[17] and the summation is over all rovibrational states *i* of the reactant, with E_i being the energy and g_i the relative population of the reactant in this state ($\Sigma g_i = 1$). The number of rovibrational states was counted using molecular parameters taken from quantum chemical calculations described below and the Beyer-Swinehart-Stein-Rabinovitch algorithm.[24-26] The relative population of states g_i was determined assuming a Boltzmann distribution at 300 K.

Equation (4) works well in cases where the rate constant for dissociation is fast compared to the experimental time τ between collisional excitation and product detection. With increasing molecular size, more rovibrational states are available to distribute the excitation energy and dissociation becomes slower.[27] In our apparatus, the experimental time available is $\tau \approx 5 \times 10^{-4}$ s. Therefore, data were modeled using Rice-Ramsperger-Kassel-Marcus (RRKM) statistical

theory[27-29] to account for the kinetic shift of the energy threshold. The total reaction cross section is then given as

$$\sigma_j(E)=\left(\frac{N\sigma_{0,j}}{E}\right)\sum_i g_i \int_{E_{0,j}-E_i}^{E} \frac{k_j(E_i^*)}{k_{tot}(E_i^*)}(E-\varepsilon)^{N-1}P_{D1}d\varepsilon \quad (5)$$

with ε being the collision energy deposited into internal modes of the reactant so that the total energy available is $E_i^* = \varepsilon + E_i$, while $P_{D1} = 1 - \exp[-k_{tot}(E_i^*)\tau]$ is the probability of dissociation, and $k_{tot}(E_i^*)$ is the total unimolecular dissociation rate constant defined by eq 6.

$$k_{tot}(E_i^*)=\sum_j k_j(E_i^*)=\sum_j d_j N_j^{\dagger}(E_i^*-E_{0,j})/h\rho(E_i^*) \quad (6)$$

Here, $k_j(E_i^*)$ is the unimolecular rate coefficient for channel j, d_j is the corresponding reaction degeneracy, $N_j^{\dagger}(E_i^* - E_{0,j})$ is the sum of rovibrational states of the transition state (TS), and $\rho(E^*)$ is the density of states for the energized molecule. When the total reaction rate is fast compared to the experimental time τ, the integration in eq 5 leads to eq 4. Water loss from iron hydroxide cation complexes was assumed to occur through a loose TS as has been applied successfully for other metal hydroxide cations[14,15] and was treated in the phase space limit (PSL).[30]

As the $FeOH^+(H_2O)$ complex can lose either the hydroxide group or the water molecule, competitive modeling was applied for these two channels,[31] and is treated naturally by the $k_j(E_i^*)/k_{tot}(E_i^*)$ term in eq 5. Consecutive water losses from clusters with n = 2 – 4 were modeled with a sequential model.[32] In the latter case, an additional probability has to be introduced to eq 5 to describe the probability of the sequential dissociation:

$$P_{D2} = 1 - \exp[-k_2(E_2^*)]\tau. \quad (7)$$

Here, $E_2^* = E_i^* - E_{0,j} - T_1 - E_L$ corresponds to the internal energy of the primary product ion available for further dissociation and k_2 to the rate constant of this process. T_1 and E_L are the translational energy of the primary products and the internal energy of the neutral product, respectively. These two values are estimated using statistical approaches.[32] All other parameters of the modeling input, for the energized molecule as well as the products, are taken from quantum chemical calculations described below. The model cross sections of eq 5 were convoluted over the kinetic energy distributions of both reactants before comparing with experimental cross sections. A nonlinear

least-squares procedure was applied to vary the fitting parameters $\sigma_{0,j}$, N, and $E_{0,j}$ to match the data throughout the threshold region.

The $E_{0,j}$ parameter corresponds to the 0 K BDE between the ligand and the remaining iron complex. In case of sequential dissociation, the BDE for the secondary water loss corresponds to the difference between the energy thresholds for primary and secondary water loss. Uncertainties in the reported BDEs were calculated by fitting eight data sets corresponding to zero pressure extrapolated cross sections for each reactant ion and varying the calculated vibrational frequencies by ± 10%, the factor N by ± 0.1, and the experimental time τ by a factor of 2. In addition, an absolute uncertainty of 0.05 eV in the kinetic energy in the lab frame was taken into account.

Computational Details

The Gaussian16 computation package[33] was used to determine ground state multiplicities and geometries of $FeOH^+(H_2O)_n$ and $Fe^+(H_2O)_n$ complexes at a B3LYP/6-311+G(d,p) level of theory.[34-36] The same level was used to compute vibrational frequencies and rotational constants. Frequencies were scaled by 0.989[37] before being used for data modeling as well as for the zero-point energy (ZPE) and thermal corrections. Single point (sp) calculations were performed without further geometry optimization at B3LYP, B3P86,[38] MP2(full),[39] and CCSD(T,full)[40-43] levels with a 6-311+G(2d,2p) basis set (where full indicates correlation of all electrons). In addition, a reoptimization of the low-energy B3LYP/6-311+G(d,p) geometries was performed using a def2-TZVP basis set with the Coulomb attenuation method cam-B3LYP[44] functional, a treatment paralleling that of Garand and co-workers.[9] For the lowest energy structures, empirical dispersion corrections were also considered using the GD3BJ approach.[45,46] Although several approaches were tested, we report values at the B3LYP-GD3BJ/6-311+G(2d,2p)//B3LYP-GD3BJ/6-311+G(d,p) and cam-B3LYP-GD3BJ/def2-TZVP levels including zero point energies (scaled by 0.989).[37] For $FeOH^+(H_2O)_n$ complexes, results at a MP2(full)/pwCVTZ//B3LYP-GD3BJ/pwCVTZ level were found to provide favorable bond energies. The pwCVTZ basis set refers to the use of aug-cc-pVTZ on O and H[47,48] and the aug-cc-pwCVTZ-NR basis set on Fe,[49] which is

an all-electron, nonrelativistic weighted core/valence basis set including diffuse and polarization functions, as obtained from the EMSL basis set site.[50] For $Fe^+(H_2O)_n$ species, MP2(full) and CCSD(T,full) results were obtained using the 6-311+G(2d,2p) basis set and B3LYP-GD3BJ/6-311+G(d,p) geometries and vibrational frequencies. As a last step, basis set superposition error (BSSE) corrections in BDEs were calculated at the full counterpoise limit for the lowest energy structures.[51]

The generation of input geometry structures was guided by chemical intuition, by structures described in literature for $FeOH^+(H_2O)_n$,[9] and by geometries known for other transition metal hydroxide complexes, $CoOH^+(H_2O)_n$ and $CuOH^+(H_2O)_n$.[14,15] To compare the experimental and theoretical results for $FeOH^+(H_2O)_n$ presented in this work with $Fe^+(H_2O)_n$ BDEs, the latter were also computed for $Fe^+(H_2O)_n$ at the same levels of theory as used for the hydroxide species. Geometry input structures for the optimizations were generated on the basis of work by Ohashi et al., who discussed geometrical structures of $Fe^+(H_2O)_n$ with n = 1 – 8 in detail.[52] Their calculations used B3LYP with a 6-311+G(2df) basis set for iron and 6-31+G(d) for O and H. For both $FeOH^+(H_2O)_n$ and $Fe^+(H_2O)_n$ systems, we do not claim to have identified all low-lying isomers but an effort has been made to find as many as possible.

RESULTS

General Theory Considerations

The ground state (GS) of the atomic iron cation is ^6D with the ^4F state lying 24.3 kJ/mol higher in energy considering the average over all spin-orbit levels.[53] Unfortunately, all levels of theory used here, except for CCSD(T), fail to predict this correctly, resulting in the ^4F state lying 16 – 40 kJ/mol lower. Our CCSD(T)/6-311+G(2d,2p) calculations give an accurate value of 25.6 kJ/mol, in agreement with similar results in the literature.[54] This failure of DFT and MP2 has been reported in the literature[52,55-59] and resolved through the use of ECPs by Glukhovtsev, Bach and Nagel,[55] the development of DFT optimized contracted Gaussian basis sets for the first row transition metals called $DZVP_{opt}$ by Chiodo et al.,[57,58] or the inclusion of scalar relativistic effects

by Altun et al.[59] The latter analyzed the influence of scalar relativistic effects using Douglas-Kroll-Hess 2nd order scalar relativistic (DKH2) corrections on their B3LYP calculations of Fe^+ and found the sextet state strongly stabilized by 29 – 33 kJ/mol, depending on the basis set. While B3LYP alone in combination with various basis sets (B1, B2, 6-311++G(3df,p), TZVPP, cc-pVQZ, def2-QZVPP) usually yielded the quartet state as GS by 8.4 to 20.9 kJ/mol, the inclusion of DKH2 led to the sextet state being favored by 14.2 kJ/mol (with cc-pVQZ) and 17.0 kJ/mol (with def2-QZVPP). Bauschlicher et al. have shown that the correct spin GS can be calculated by implementing more polarization functions; however, this improvement does not work for B3LYP.[56]

When a water ligand is added to Fe^+, the present B3LYP/6-311+G(2d,2p) calculations predict a quartet spin state as the $Fe^+(H_2O)$ GS with the sextet state lying 40.0 kJ/mol higher. This result agrees with results of Garza-Galindo et al., who used B3LYP/$DZVP_{opt}$ to find the sextet state of $Fe^+(H_2O)$ is 42 kJ/mol higher than the quartet.[60] In contrast, Altun et al.[59] predict the sextet state to be lower by 28.0 kJ/mol using their benchmark CCSDT(Q) and scalar relativistic approach. This result agrees with our current CCSD(T) calculations, which find the sextet state to be lower by 12.9 kJ/mol. Therefore, for all other levels of theory, the present work corrects for the discrepancy in the Fe^+ spin state compared to experiment by computing BDEs on both the quartet and sextet surfaces and determining the relative energies of $Fe^+(H_2O)_n$, n = 1 – 2, by moving the $Fe^+(H_2O)_{n-1}$ + H_2O product asymptotes to match experiment. This correction was originally suggested by Ricca and Bauschlicher who then find that the sextet state is the GS by 5.4 (B3LYP) or 3.3 (MCPF) kJ/mol.[62] This procedure is illustrated by an exemplary potential energy diagram for the dissociation of $Fe^+(H_2O)_2 \rightarrow Fe^+(H_2O) + H_2O \rightarrow Fe^+ + 2\ H_2O$ given in Figure S1 of the Supporting Information. At the B3LYP/6-311+G(2d,2p) level, this correction indicates that the sextet state of $Fe^+(H_2O)$ lies 5.3 kJ/mol lower than the quartet state, in agreement with the CCSD(T) and CCSDT(Q) results. For $Fe^+(H_2O)_2$ on the other hand, we find that the quartet state is significantly lower (by 62.1 kJ/mol at this level) compared to the sextet state. This result is again consistent with previous work: Ricca and Bauschlicher find a corrected separation of only 5.4

kJ/mol,[62] whereas Garza-Galindo et al. found the sextet state 92 kJ/mol higher than the quartet.[60] BDEs for pure quartet and sextet surfaces are presented in the Supporting Information, Table S1. The addition of further water molecules leads to a stabilization of the quartet state and increases the energy gap towards the sextet. Similar behavior is observed for other levels of theory, as detailed further below.

In the case of $FeOH^+$, we find that the addition of the hydroxide group to Fe^+ leads to a quintet GS, which lies 118.5 kJ/mol lower than the triplet state for B3LYP/6-311+G(2d,2p). Other levels of theory show similar results. Glukhovtsev et al. also reported a quintet GS but do not report the exact energy difference.[55] Notably, the failure of DFT and MP2(full) methods to predict the correct GS of Fe^+ and $Fe^+(H_2O)$ should have no impact on BDEs for the water loss from $FeOH^+(H_2O)_n$ species, but is relevant for OH loss, as discussed further below.

Computational Results for $FeOH^+(H_2O)_n$ with n = 1 - 4

Relative energetics for the different geometrical isomers of the $FeOH^+(H_2O)_n$ clusters at 0 and 298 K are reported in Table 1. GS geometries determined through B3LYP/6-311+G(d,p) geometry optimizations are shown in Fig. 1 with geometrical parameters listed in Table 2. To describe a particular structure, a (x,y) nomenclature is used where x represents the number of water molecules bound directly to the iron in the first solvation shell while y stands for the number of water molecules in the second solvation shell. To specify whether a water molecule bound through hydrogen bonds functions as donor or acceptor, a D/A denotation is used. The denotation carries an OH subscript in case the hydrogen bond is between the hydroxide and a water molecule instead of between two water molecules.

For $FeOH^+(H_2O)$, the GS isomer is (1,0) in which the water binds to the iron cation. The Fe^+-OH bond length is unperturbed by addition of the water ligand, whereas the FeOH angle becomes more linear upon water complexation, Table 2. Unsurprisingly, the water ligand is bound at a longer distance than the covalently bound hydroxide (by 0.29 Å). There is a nearly linear OFeO arrangement with the hydroxide group hydrogen lying perpendicular to the plane defined

by the water molecule and the iron, such that the symmetry of this molecule is C_s ($^5A'$ state). This is in contrast to structures reported for $CoOH^+(H_2O)$ and $CuOH^+(H_2O)$, where all hydrogens lie in the same plane.[14,15] Interestingly, as the FeOH bond angle in $FeOH^+(H_2O)$ moves to linearity, so does the OFeO bond angle. A TS is located at ∠FeOH = 180.0° and ∠OFeO = 180.0° with an imaginary frequency of 76 cm^{-1} corresponding to the HOFe bend perpendicular to the plane defined by the H_2O ligand. This TS lies only 0.03 kJ/mol above the bent GS species *before* zero-point energy corrections and 0.8 kJ/mol below afterwards. Thus, the molecule resides in a double-well potential in the out-of-plane bend, but the zero-point energy exceeds the barrier such that the FeOH and OFeO angles are actually linear. This linearity permits the lone pair electrons on both oxygen atoms to donate into both singly occupied dπ orbitals on the iron. The only other isomer found for n = 1 is (0,1)_A_{OH} in which the water ligand binds to the hydroxide instead of the iron. This isomer shows a very large relative energy compared to the GS of > 133 kJ/mol at 0 K (Table 1) and is therefore not discussed further.

Additional water molecules are favorably bound directly on the iron atom for up to three molecules. The (2,0) GS isomer of $FeOH^+(H_2O)_2$ has an almost planar geometry (∠OFeOO dihedral angle ~ 175°) with regard to the heavy atoms, but is asymmetric with water ligands at ∠HO-Fe-O angles that differ by 32°. This is consistent with the analogous (2,0) GS complexes for Cu and Co.[14,15] In the (1,1)_A structure, one of the water ligands binds to the first shell water ligand to form a second shell. This species lies above the GS by 25 – 38 kJ/mol. If the second shell water binds to the hydroxide, (1,1)_A_{OH}, B3LYP predicts two nearly degenerate structures distinguished by a nearly free rotation of the first-shell water molecule only. The dihedral angles spanned by the HO···OH atoms belonging to the water molecules are either 81.2°, which is denoted 'staggered' (s), or 11.5°, which is denoted 'eclipsed' (e). The deviation from 90° and 0°, respectively, is a result of the non-linear ∠FeOH angle.

For n = 3, the (3,0) GS has a trigonal pyramidal structure with respect to the oxygen atoms that is strongly deformed by long-range (2.63 – 3.01 Å) hydrogen bonds between water molecules as well as one water ligand and the hydroxide group. In the analogous complexes of Cu and Co,

(3,0) is the most favorable isomer as well, although Cu shows a square planar structure,[15] while $CoOH^+(H_2O)_3$ is a distorted tetrahedron.[14] For $FeOH^+(H_2O)_3$, there are three (2,1) structures with a second shell water ligand bound to either two (AA) or one (A) inner shell water ligands or to the hydroxide group (A_{OH}). The (2,1)_AA and _A structures lie 15 – 30 kJ/mol above the (3,0) GS, whereas A_{OH} lies 49 – 68 kJ/mol higher, Table 1.

For n = 4, a distinction has to be made between the ground structure at 0 and 298 K. The (3,1)_AAD_{OH} isomer represents the GS at 0 K at all levels of theory except for CCSD(T) where (3,1)_AAD_{OH} and (4,0)_$D_{OH,b}$ are basically degenerate. At 298 K, the lowest energy isomer is (3,1)_A for B3LYP and B3P86, (4,0)_$D_{OH,a}$ for MP2(full), (4,0)_$D_{OH,b}$ for CCSD(T), (3,1)_AD_{OH} for cam-B3LYP (with and without GD3BJ), and (3,1)_AA for B3LYP-GD3BJ. The (3,1)_AAD_{OH} isomer is the first 0 K GS to have a water molecule in the second solvation shell, where it is threefold anchored by accepting hydrogen bonds from two inner shell water molecules and donating a hydrogen bond to the hydroxide ligand. This constrains the outer shell water molecule leading to C_s symmetry, which also means that this isomer is entropically less favorable. The (3,1)_A isomer is more favorable at 298 K because the water in the outer shell is bound to only one inner shell water molecule. This enables rotation of the outer shell water and the entropic contribution favors this isomer by ~11 kJ/mol compared to (3,1)_AAD_{OH}. The MP2(full) and CCSD(T) levels of theory predict the (4,0)_$D_{OH,a}$ and (4,0)_$D_{OH,b}$ isomers, respectively, as the GS at 298 K where the oxygen atoms form a trigonal bipyramid deformed by hydrogen bonding interactions between the ligands. One of the axial water ligands hydrogen binds to the hydroxide. The two variants of the (4,0) structure differ only by orientation of the water ligands (rotations of two ligands by 90°). At most levels of theory, these lie within 1 kJ/mol at 0 K with only CCSD(T) and cam-B3LYP-GD3BJ predicting larger differences, 2.4 and 4 kJ/mol, respectively. At 298 K, the (4,0)_$D_{OH,b}$ variant lies 0.7 – 4.0 kJ/mol above the (4,0)_$D_{OH,a}$ structure. The structures (3,1)_AD_{OH} and (3,1)_AA have relative energies that are close to the isomers discussed so far. Both isomers hold the outer shell water molecule through two hydrogen bonds: either by accepting

one from one inner shell water and donating one hydrogen bond to the hydroxide group, or by accepting both hydrogen bonds from two inner shell waters.

Overall, the addition of water molecules to the $FeOH^+$ species leads to an increasing Fe-OH bond length, starting at 1.71 Å and reaching 1.83 Å for n = 4, Table 2. The ∠FeOH angle varies with the specific isomers but tends to be more linear when no interactions with water molecules are present because short and long-range hydrogen bonds lead to a compressed geometry. Geometries found at the B3LYP-GD3BJ level were very similar to those found by B3LYP, with bond lengths generally within 0.01 Å and bond angles within 1°. Minor geometry differences were found between geometry optimized B3LYP and cam-B3LYP structures, mostly associated with rotations of water molecules. To estimate the differences in energy that such variations produced, single point calculations at the cam-B3LYP/def2-TZVP level of theory were performed on the geometries optimized with B3LYP/6-311+G(d,p). The strongest energy decrease of these sp calculations compared to the reoptimized geometry was found to be 5.6 kJ/mol. The minor changes in geometries between the different levels of theory can therefore be neglected for the calculation of BDEs.

In their exploration of the $FeOH^+(H_2O)_n$ (n = 1 – 4) complexes, Marsh et al. used D_2 tagging at about 10 K to spectroscopically investigate these species in the OH stretching region (2700 – 3800 cm^{-1}).[9] For n = 1 – 3, experimental spectra agreed well with those calculated at the cam-B3LYP/def2-TZVP level for the (1,0), (2,0), and (3,0) structures, the same GS isomers found here. For n = 4, they concluded that the (3,1)_AAD_{OH} and (3,1)_AA isomers were predominantly present with a possible minor contribution from the (4,0) structure. They explicitly eliminate the presence of the (3,1)_AD_{OH} isomer experimentally because this isomer should have an intense band at ~2600 cm^{-1} (2725 cm^{-1} in our B3LYP/6-311+G(d,p) results), and no intensity in this region is observed. Although they did not consider the (3,1)_A isomer, it is predicted to have an intense band around 3100 cm^{-1}, which is inconsistent with experiment. On the basis of the energetics alone, the theoretical results predict that only the AAD_{OH} structure would be populated at 10 K; however, this is also the most entropically disfavored structure such that contributions from other structures

are feasible. In our experiment, where the ions are formed at room temperature, different levels of theory make different predictions, but the relatively low 298 K Gibbs energies suggest that all six of these isomers could exist in equilibrium.

Computational Results for $Fe^+(H_2O)_n$ with n = 1 - 4

The geometrical GS structures for $Fe^+(H_2O)_n$ have been studied theoretically as well as experimentally by various groups.[52,60-62] We present here the theoretical results using the same levels of theory as for the hydroxides, which are needed for the comparison to experimental BDEs for hydroxide loss from $FeOH^+(H_2O)_n$. The energies of low-lying isomers are summarized in Table 3, and because the structures have been published before, these are included in Figure S2 of the Supporting Information. Overall, we find good agreement of our geometry structures with those published by Ohashi et al.[52] (The only exception is their 3II isomer, (2,1)_AA, which converges to the (3,0) isomer at B3LYP/6-311+G(d,p) and cam-B3LYP/def2-TZVP levels of theory.) Most levels of theory suggest that the third and fourth water ligands are bound in the second shell rather than directly to the metal, in contrast with earlier calculations of Ricca and Bauschlicher[62] (who did not examine the second shell geometries). Oddly, MP2//B3LYP results indicate the (4,0) geometry is most stable by a large amount (86 kJ/mol), which is undoubtedly anomalous as concurrently calculated CCSD(T)//B3LYP results as well as MP2//B3LYP-GD3BJ results are more similar to the various DFT approaches, Table 3. Notably, several levels of theory suggest that at 298 K, there are three structures that could be populated for n = 4: (2,2)_2D_2A, (2,2)_DD_2A, and (3,1)_D_A. This result is potentially consistent with the IR spectra of $Fe^+(H_2O)_4$ taken by Ohashi et al.[52]

Experimental and Thermochemical Results

The threshold collision-induced dissociation (TCID) technique was applied to determine CID cross sections for water loss from $FeOH^+(H_2O)_n$ species with n = 1 – 4 and the loss of the neutral OH group from $FeOH^+(H_2O)$ upon collision with Xe. Exemplary CID cross sections versus

E_{CM} and E_{Lab} acquired at a collision gas pressure of about 0.2 mTorr are presented in Fig. 2. Figure 2 shows that, as the size of the complex decreases, the apparent thresholds for loss of one water ligand gradually increase and the magnitude of the total cross section decreases. For complexes with two and more water molecules, we observe the sequential loss of water as the collision energy is increased. For the $FeOH^+(H_2O)$ complex, loss of the OH ligand is observed at a much higher energy than loss of the H_2O ligand, but OH loss is not observed for the larger complexes, presumably because the intensity of this product is too small to detect. Notably, as shown in Fig. 2a, $FeOH^+(H_2O)_4$ has a nonzero probability to dissociate at room temperature even at a collision energy of 0 eV. This explains why no $FeOH^+(H_2O)_5$ clusters were detected under our experimental source conditions.

A collision gas pressure of 0.2 mTorr was the highest pressure used during experiments and lies well in the range of single collision conditions. Nevertheless, the cross sections show a modest dependence on the Xe gas pressure and were therefore extrapolated to zero pressure conditions before analysis to determine energy thresholds. The zero-pressure extrapolated cross sections and models of the data according to eq 5 are presented in Fig. 3. The modeling parameters including 0 K energy thresholds, as well as the activation entropy at 1000 K, $\Delta S^{\ddagger}_{1000}$,[63-65] are summarized in Table 4. We note that $\Delta S^{\ddagger}_{1000}$ is positive in all cases, consistent with the loose transition state[66] assumed for the dissociation model. Only the $\Delta S^{\ddagger}_{1000}$ values for the dissociation of $FeOH^+(H_2O)$ to $FeOH^+ + H_2O$ (10 ± 9 J/Kmol) or $Fe^+(H_2O) + OH$ (12 ± 9 J/Kmol) are relatively small.

For the primary water loss channel for the n = 2 – 4 complexes, the data are analyzed both by modeling the total cross section, which generally gives the most precise result for the threshold of a primary water loss, and the use of the sequential model that includes both primary and secondary water loss channels. As seen in Table 4, the threshold values for the primary water loss channel obtained by these two models are the same within the uncertainties. When modeling the total cross sections, we also determined thresholds when lifetime effects were not included, yielding thresholds that are shifted towards higher energies by only 0.02 – 0.03 eV. For n = 1, the

two product channels were modeled simultaneously using a competitive model, yielding 2.35 ± 0.07 eV for loss of the water ligand and considerably more energy, 4.36 ± 0.16 eV, for loss of OH.

The differences between the second and first threshold in the sequential model represent the BDEs of the secondary water loss, which compare well with those from the analyses of just the primary losses. For n = 2, this difference is 2.40 ± 0.06 eV, in good agreement with the value determined from the primary dissociation of $FeOH^+(H_2O)$, 2.35 ± 0.07 eV. Likewise, the sequential model of $FeOH^+(H_2O)_3$ gives a threshold difference of 1.39 ± 0.07 eV, agreeing well with the 1.37 ± 0.09 eV value from modeling the total cross section of $FeOH^+(H_2O)_2$. For n = 4, the difference in primary and secondary thresholds in the sequential model yields a BDE for $FeOH^+(H_2O)_3$ of 1.08 ± 0.03 eV, somewhat higher than the threshold of 0.94 ± 0.05 eV obtained by analyzing the primary water loss from this complex. As discussed above for n = 4, different structure isomers are predicted to be present at room temperature depending on the level of theory used. Therefore, we modeled the data using molecular parameters for all possible 298 K GS isomers and Table 4 reports an average of all of these fitting parameters and the uncertainties reflect these variations as well.

DISCUSSION

Comparison of Experimental and Theoretical Bond Dissociation Energies of $FeOH^+(H_2O)_n$

Experimental BDEs for water loss from $FeOH^+(H_2O)_n$ are compared to theoretically calculated values at 0 K including basis set superposition error corrections in Table 5. Counterpoise corrections do not change the energetic order of the low-lying isomers so that only the GS is considered here. For $FeOH^+(H_2O)_4$, the 298 K GS species (see Table 1) are used to calculate the 0 K BDEs at each respective theory level as these should correspond to the experimentally measured species. In all cases, theoretically predicted BDEs underestimate the experimental results for n = 1 and 2, by 14 – 36 ± 7 and 8 – 25 ± 9 kJ/mol, respectively. Cam-B3LYP-GD3BJ calculations provide results that are closest to experimental with the value for n = 2 within experimental uncertainty. For n = 3 and 4, reasonably good agreement is found, with

deviations of -10 – +7 ± 5 and -2 – 22 ± 4 kJ/mol. MP2(full), CCSD(T), and B3LYP-GD3BJ calculations are within experimental uncertainty for n = 3, whereas B3LYP and B3P86 show the best results for n = 4. Overall, theory predicts these hydration BDEs reasonably well with a mean absolute deviation (MAD) with the primary experimental values between 13 – 18 kJ/mol, with cam-B3LYP-GD3BJ being the lowest. As the secondary BDEs are systematically larger than the primary values, the MADs increase compared with these values. The use of empirical dispersion corrections during geometry optimization results in somewhat better reproduction of the experimental values, with MADs of 13 – 14 kJ/mol compared to 13 – 18 kJ/mol when based on geometries found without dispersion corrections.

Comparison of Experimental and Theoretical Bond Dissociation Energies of $Fe^+(H_2O)_n$

As discussed in the next section, the loss of OH from the $FeOH^+(H_2O)$ complex can be combined with literature values for $D_0[(H_2O)_{n-1}Fe^+-H_2O]$ to determine dehydroxylation energies of the $FeOH^+(H_2O)_n$ complexes. Therefore, we theoretically evaluated the hydration energies of $Fe^+(H_2O)_n$ for comparison to the experimental results of Dalleska et al.,[8] Table 6. As discussed above, DFT methods tend to predict the wrong spin GS for Fe^+ and $Fe^+(H_2O)$ unless relativistic effects or special basis sets are used. Therefore, except for CCSD(T) results, theoretical values for n = 1 and 2 have been adjusted so that the asymptotic energies agree with experiment for Fe^+. Further, a cursory examination of the theoretical results obtained at the MP2 level show large deviations from the other theoretical results and include anomalously large BSSE corrections. The fact that the related CCSD(T) results are reasonable suggests that the MP2 results for these systems are inaccurate because of inadequate treatment of correlation effects. Therefore, the MP2 results are not included in the discussion below.

For $Fe^+(H_2O)$, all theoretical BDEs correspond to dissociation of a sextet state to the $Fe^+(^6D)$ + H_2O GS of the products. (Table S1 lists the quartet BDEs for comparison.) The theoretical values span a range of 125 – 149 kJ/mol, with several values agreeing with the experimental value of 128.3 ± 4.8 kJ/mol within experimental uncertainty. Theoretical literature

values include those from Ricca and Bauschlicher (139.7 kJ/mol),[62] Altun et al. (140.6 kJ/mol using B3LYP/cc-pVQZ including DKH2 (B3LYP/def2-QZVPP) and ZPE (B3LYP/TZVPP) corrections, see discussion above),[59] and Garza-Galindo et al. (144.8 kJ/mol using B3LYP/DZVPopt).[60]

Notably, the BDE for the second water ligand (164.0 ± 3.9 kJ/mol) is larger than the first, which was first explained by Ricca and Bauschlicher[62] and is a result of sd hybridization. Most theoretical values (149 – 158 kJ/mol) are in reasonable agreement although generally slightly below this, with the cam-B3LYP results (171 kJ/mol with and 168 kJ/mol without empirical dispersion) being slightly higher. Garza-Galindo et al.[60] reported a BDE of 191.2 kJ/mol and Ricca and Bauschlicher[62] of 161.1 kJ/mol for one water loss from $Fe^+(H_2O)_2$. Theoretical values for n = 3 are similar, slightly lower for most levels (by 7 – 16 kJ/mol) with cam-B3LYP matching the experimental value. For n = 4, most levels of theory agree with experiment within the experimental uncertainty, but now cam-B3LYP values are high by 19 – 22 kJ/mol. Ricca and Bauschlicher report BDEs for n = 3 and 4 of 62.3 and 48.1 kJ/mol, although they only considered the (3,0) and (4,0) structures. Overall, the comparisons between the present calculations and experiment are reasonable with MADs ranging from 8 – 12 kJ/mol for the various DFT and CCSD(T) levels.

Dehydroxylation of $FeOH^+(H_2O)_n$

The $FeOH^+(H_2O)$ complex was the only species where the OH loss was experimentally observed. Here, the $(H_2O)Fe^+$-OH BDE is measured as 4.36 ± 0.16 eV (420.7 ± 15.4 kJ/mol). Nevertheless, it is possible to obtain hydroxide BDEs for other $FeOH^+(H_2O)_n$ species using the thermodynamic cycle shown in Figure 4, which shows the relation expressed in eq 8.

$$D_0[(H_2O)_nFe^+\text{-}OH] = D_0[(H_2O)_{n-1}FeOH^+\text{-}OH_2] + D_0[(H_2O)_{n-1}Fe^+\text{-}OH] - D_0[(H_2O)_{n-1}Fe^+\text{-}OH_2] \quad (8)$$

This calculation requires the hydration energies of Fe^+, as discussed in the previous section. These experimental BDEs are given in Fig. 4 together with the experimental BDEs for water loss from $FeOH^+(H_2O)_n$ obtained in the current work. From these values, BDEs for the loss of the OH group

from the $FeOH^+(H_2O)_n$ complexes with n = 0, 2 – 4 are derived. As can be seen in this figure, BDEs for losing a water molecule from $FeOH^+(H_2O)_n$ have similar magnitudes to those for losing water from $Fe^+(H_2O)_n$. Only the loss of water from $FeOH^+(H_2O)$ has a significantly higher BDE of 226.7 ± 7.1 kJ/mol compared to 128.3 ± 4.8 kJ/mol for $Fe^+(H_2O)$. The latter bond is particularly weak because the water ligand interacts repulsively with the 6s electron of $Fe^+(^6D, 4s^13d^6)$. Because this electron is involved in the covalent bond between Fe^+ and OH, this repulsive interaction is essentially removed.

The BDE determined here for the Fe^+-OH loss is 322.3 ± 17.6 kJ/mol, which can be compared with several values in the literature. Murad used high temperature mass spectrometry and ionization energy measurements to determine $D_0(Fe^+\text{-OH})$ = 318 ± 19 kJ/mol.[67] Cassady and Freiser[68] measured the relative proton affinity of FeO to yield $D_0(Fe^+\text{-OH})$ = 322 ± 25 kJ/mol and a photodissociation threshold of $D_0(Fe^+\text{-OH})$ = 305 ± 13 kJ/mol. Clearly, these values are all nicely consistent. In contrast, Michl and coworkers[69] used a CID approach to obtain $D_0(Fe^+\text{-OH})$ = 357 ± 19 kJ/mol, although they note that dissociation to the $Fe^+(^4F)$ excited asymptote might elevate their value by this excitation energy, 24 kJ/mol. This would lower their result to match the previous experiments and the current result within experimental uncertainty. Support for the higher value of Michl and coworkers came from our laboratory, Clemmer et al.,[70] which reported a value of 366 ± 12 kJ/mol. However, this value is cited from unpublished work (which in fact was never published). If published threshold values from the work of Clemmer et al. are used, the $Fe^+(^4F) + D_2O \rightarrow FeOD^+ + D$ reaction leads to $D_0(Fe^+\text{-OH})$ = 343 ± 21 kJ/mol and the $FeO^+ + D_2 \rightarrow FeOD^+ + D$ reaction leads to $D_0(Fe^+\text{-OH})$ = 290 ± 8 kJ/mol (using an updated value of $D_0(Fe^+\text{-O})$ = 340 ± 2 kJ/mol[71]), where the latter $FeOH^+$ BDE may be low because competition with more favorable channels was not included in the data analysis. Consideration of all of these results suggests that the value obtained in the current study is among the more accurate values, agreeing nicely with the seminal work of Murad.

The $(H_2O)_nFe^+$-OH BDEs derived here are compared to theoretical values in Table 7. Because these involve formation of $Fe^+(H_2O)_n$, the theoretical values for n = 1 and 2 must again

be corrected for the experimentally correct asymptote associated with the $Fe^+(^6D)$ GS. MP2 values are not considered reliable for the same reasons discussed above for the $Fe^+(H_2O)_n$ species. For $FeOH^+$, the theoretical BDEs vary between 318 – 335 kJ/mol, all in good agreement with the 322.3 ± 17.6 kJ/mol value derived experimentally. Glukhovtsev et al. calculated a value of 350.6 kJ/mol using an ECP and (8s7p6d2f)/[6s5p4d2f] valence basis set for the Fe cation.[55] The iron hydroxide bond is stabilized by additional water molecules, rising to experimental values of 389 – 421 kJ/mol, with n = 1 providing the strongest and n = 2 the weakest of these. Theory reproduces this general trend but generally underestimates the BDEs for n = 1 – 4 by 16 – 55 kJ/mol. The MADs cover a comparable range, 25 – 40 kJ/mol, with CCSD(T) providing the best overall results. The origins of these deviations are not immediately clear, but they are also not unique. For the comparable $(H_2O)_nCo^+$-OH BDEs, theory performed at the same levels (except CCSD(T)) yields MADs of 15 – 38 kJ/mol.[14]

CONCLUSION

Guided ion beam tandem mass spectrometry is used to measure the dissociation energies of hydrated iron hydroxide cations. Direct measurements of the hydration energies are obtained by threshold collision-induced dissociation of $FeOH^+(H_2O)_n$ with Xe. The hydration energies gradually decrease from n = 1 to n = 4, spanning a range from 227 – 59 kJ/mol. The $FeOH^+(H_2O)$ complex is also observed to dissociate by loss of the hydroxyl ligand, thereby allowing direct measurement of the $(H_2O)Fe^+$-OH bond energy as well. This BDE is combined with the hydration energies and literature bond energies for $Fe^+(H_2O)_n$, where n = 1 – 4, to extract experimental values for the dehydroxylation energies of $FeOH^+(H_2O)_n$, n = 0, 2 – 4, complexes as well. Here, the values remain relatively constant, between 389 and 421 kJ/mol for n = 1 – 4. The value obtained for $D_0(Fe^+$-OH), 322 ± 18 kJ/mol, agrees well with several other previous experimental values. Except for this bond energy, all other BDEs obtained in this work are the first experimental determinations.

To better understand the trends in this thermochemistry, extensive theoretical explorations of the $FeOH^+(H_2O)_n$ and $Fe^+(H_2O)_n$ complexes were performed at multiple levels of theory. For the hydration energies of $FeOH^+$, theory is somewhat low for n = 1 and 2, and accurate for n = 3 and 4, with overall MADs from experiment of 13 – 18 kJ/mol. In calculating the hydration energies of Fe^+, all theoretical results except CCSD(T) calculations must be corrected for the inability of theory to predict the correct ground electronic state of Fe^+, but this failure can be overcome by calculating results on both quartet and sextet spin surfaces and correcting to experimental energetics. Once this is done, theoretical values for the hydration energies of the iron hydroxide cation are reproduced reasonably well with MADs of 8 – 12 kJ/mol (excluding MP2 results, which are anomalous). Finally, theory also reproduces the Fe^+-OH bond energy measured here and elsewhere, but predicts OH bond energies to $Fe^+(H_2O)_n$ complexes that are considerably lower than the experimental values. The origins of this failure are not clear.

ASSOCIATED CONTENT

Supporting Information

An exemplary potential energy diagram for the dissociation of $Fe^+(H_2O)_2$ including the spin state corrected energy surface is presented together with a table showing all theoretical 0 K BDEs for the different spin surfaces with and without counterpoise corrections. Also included are a figure showing the geometries of the $Fe^+(H_2O)_n$ GS isomers, with n = 0 – 4, optimized at the B3LYP/6-311+G(d,p) level of theory.

AUTHOR INFORMATION

Corresponding Author

*armentrout@chem.utah.edu

ORCID

P. B. Armentrout: 0000-0003-2953-6039

Notes

The authors declare no competing financial interest.

ACKNOWLEDGMENTS

Financial support for this project was provided by the National Science Foundation, Grant No. CHE-1664618. Computing resources were generously provided by the Center for High Performance Computing (CHPC) at the University of Utah. O. S. thanks the Verband Der Chemischen Industrie gratefully for scholarship funds, R. A. Coates and C. P. McNary for experimental advice, and R. Schäfer for helpful discussions.

REFERENCES

[1] Holleman, A. F.; Wiberg, E. *Lehrbuch der Anorganischen Chemie;* 101 Edition, de Gruyter: Berlin, 1995.

[2] Chang, R. *Physical Chemistry with Application to Biological Systems*; Second Edition, Macmillian Publishing Co., Inc.: New York, 1981.

[3] Bergethon, P. R. *The Physical Basis of Biochemistry: The Foundations of Molecular Biophysics*; Springer-Verlag, New York, 1998.

[4] Goto, K.; Tamura, H.; Nagayama, M. The Mechanism of Oxygenation of Ferrous Ion in Neutral Solution. *Inorg. Chem*. **1970**, *9*, 963-964.

[5] Cotton, F. A.; Wilkinson, G. *Advanced Inorganic Chemistry*; Third Edition, John Wiley & Son, Inc.: New York, 1972.

[6] Donald, W. A.; Leib, R. D.; Demireva, M., Negru, B.; Neumark, D. M., Williams, E. R. Average Sequential Water Molecule Binding Enthalpies of $M(H_2O)_{19\text{-}124}^{2+}$ (M=Co, Fe, Mn, and Cu) Measured with Ultraviolet Photodissociation at 193 and 248 nm. *J. Phys. Chem. A* **2011**, *115*, 2-12.

[7] O'Brien, J. T.; Williams, E. R. Coordination Number of Hydrated Divalent Transition Metal Ions Investigated with IRPD Spectroscopy. *J. Phys. Chem. A* **2011**, *115*, 14612-14619.

[8] Dalleska, N. F.; Honma, K.; Sunderlin, L. S.; Armentrout, P. B. Solvation of Transition Ion Metal Ions by Water. Sequential Binding Energies of $M^+(H_2O)_x$ (x=1-4) for M=Ti to Cu Determined by Collision-Induced Dissociation. *J. Am. Chem. Soc*. **1994**, *116*, 3519-3528.

[9] Marsh, B. M.; Voss, J. M.; Zhou, J.; Garand, E. Coordination Structure and Charge Transfer in Microsolvated Transition Metal Hydroxide Clusters $[MOH]^+(H_2O)_{1-4}$. *Phys. Chem. Chem. Phys*. **2015**, *17*, 23195-23206.

[10] Blades, A. T.; Jayaweera, P.; Ikonomou, M. G.; Kebarle, P. Ion-Molecule Clusters Involving Doubly Charged Metal Ions (M^{2+}). *Int. J. Mass Spectrom. Ion Processes* **1990**, *102*, 251-267.

[11] Shvartsburg, A. A.; Siu, K. W. M. Is There a Minimum Size for Aqueous Doubly Charged Metal Cations? *J. Am. Chem. Soc*. **2001**, *123*, 10071-10075.

[12] Hofstetter, T. E.; Armentrout, P. B. Threshold Collision-Induced Dissociation and Theoretical Studies of Hydrated Fe(II): Binding Energies and Coulombic Barrier Height. *J. Phys. Chem. A* **2013**, *117*, 1110-1123.

[13] Cooper, T. E.; Armentrout, P. B. Experimental and Theoretical Investigation of the Charge-Separation Energies of Hydrated Zinc(II): Redefinition of the Critical Size. *J. Phys. Chem. A* **2009**, *113*, 13742-13751.

[14] Coates, R. A.; Armentrout, P. B. Binding Energies of Hydrated Cobalt Hydroxide Ion Complexes: A Guided Ion Beam and Theoretical Investigation. *J. Chem. Phys.* **2017**, 147, 064305.

[15] Sweeny, A. F.; Armentrout, P. B. Guided Ion Beam Studies of the Collision-Induced Dissociation of $CuOH^+(H_2O)_n$ (n=1-4): Comprehensive Thermodynamic Data for Copper ion Hydration. *J. Phys. Chem. A* **2014**, *118*, 10210-10222.

[18] Moison, R. M.; Armentrout, P. B. An Electrospray Ionization Source for Thermochemical Investigation with the Guided Ion Beam Mass Spectrometer, *J. Am. Soc. Mass Spectrom*. **2007**, *18*, 1124-1134.

[19] Carl, D. R.; Moison, R. M.; Armentrout, P. B. In-Source Fragmentation Technique for the Production of Thermalized Ions. *J. Am. Soc. Mass Spectrom*. **2009**, *20*, 2312-2317.

[20] Carpenter, J. E., McNary, C. P.; Furin, A.; Sweeney, A. F.; Armentrout, P. B. How Hot Are Your Ions Really? A Threshold Collision Induced Dissociation Study of Substituted Benzylpiridinium "Thermometer" Ions. *J. Am. Soc. Mass Spectrom.* **2017**, *28*, 1876-1888.

[21] Carl, D. R.; Chatterjee, B. K.; Armentrout, P. B. Threshold Collision-Induced Dissociation of $Sr^{2+}(H_2O)_x$ Complexes (x = 1–6): An Experimental and Theoretical Investigation of the Complete Inner Shell Hydration Energies of Sr^{2+}, *J. Chem. Phys*. **2010**, *132*, 044303.

[22] Gerlich, D. Inhomogeneous rf Fields: A Versatile Tool for the Study of Processes with Slow Ions. *Adv. Chem. Phys.* **1992**, *82*, 1-176.

[23] Daly, N. R. Scintillation Type Mass Spectrometer Ion Detector. *Rev. Sci. Instrum*. **1960**, *31*, 264-267.

[24] Beyer, T. S.; Swinehart, D. F. Number of Multiply-Restricted Partitions. *Commun. ACM* **1973**, *16*, 379.

[25] Stein, S. E.; Rabinovitch, B. S. On the Use of Exact State Counting Methods in RRKM Rate Calculations. *Chem. Phys. Lett.* **1977**, *49*, 183-188.

[26] Stein, S. E.; Rabinovitch, B. S. Accurate Evaluation of Internal Energy Level Sums and Densities Including Anharmonic Oscillators and Hindered Rotors. *J. Chem. Phys*. **1973**, *58*, 2438-2445.

[27] Steinfeld, J. I.; Francisco, J. S.; Hase, W. L. *Chemical Kinetics and Dynamics*; Prentice-Hall: New Jersey, 1989.

[28] Gilbert, R. G.; Smith, S. C. *Theory of Unimolecular and Recombination Reactions*; Blackwell Scientific: London, 1990.

[29] Truhlar, D. G.; Garrett, B. C.; Klippenstein, S., J. Current Status of Transition-State Theory. *J. Phys. Chem.* **1996**, *100*, 12771-12800.

[30] Rodgers, M. T.; Ervin, K. M.; Armentrout, P. B. Statistical Modeling of Collision-Induced Dissociation Thresholds. *J. Chem. Phys.* **1997**, *106*, 4499-4508.

[31] Rodgers, M. T.; Armentrout, P. B. Statistical Modeling of Competitive Threshold Collision-Induced Dissociation. *J. Chem. Phys.* **1998**, *109*, 1787-1800.

[32] Armentrout, P. B. Statistical Modeling of Sequential Collision-Induced Dissociation. *J. Chem. Phys.* **2007**, *126*, 234302.

[33] Frisch, M. J.; Trucks, G. W.; Schlegel, H. B.; Scuseria, G. E.; Robb, M. A.; Cheeseman, J. R.; Scalmani, G.; Barone, V.; Petersson, G. A.; Nakatsuji, H.; et al. Gaussian 16, Revision A.03, Inc. Wallingford CT, 2016.

[34] Becke, A. D. Density-Functional Thermochemistry. III. The Role of Exact Exchange. *J. Chem. Phys.* **1993**, *98*, 5648-5652.

[35] Lee, C.; Yang, W.; Parr, R. G. Development of the Colle-Salvetti Correlation-energy Formula into a Functional of the Electron Density. *Phys. Rev. B* **1988**, *37*, 785-789.

[36] Stephens, P. J.; Devlin, F. J.; Chabalowski, C. F.; Frisch, M. J. Ab Initio Calculation of Vibrational Absorption and Circular Dichroism Spectra Using Density Functional Force Fields. *J. Phys. Chem.* **1994**, *98*, 11623–11627.

[37] Bauschlicher, C. W. Jr.; Partridge, H. A Modification of the Gaussian-2 Approach Using Density Functional Theory. *J. Chem. Phys.* **1995**, *103*, 1788-1791.

[38] Perdew, J. P. Density-Functional Approximation for the Correlation Energy of the Inhomogeneous Electron Gas. *Phys. Rev. B* **1986**, *33*, 8822-8824.

[39] Møller, C.; Plesset, M. S. Note on an Approximation Treatment for Many-Electron Systems. *Phys. Rev.* **1934**, *46*, 618-622.

[40] Cížek, J. *Adv. Chem. Phys.*; Vol. 14, Ed. P. C. Hariharan, Wiley Interscience, New York, 1969.

[41] Purvis III, G. D.; Bartlett, R. J. A Full Coupled-Cluster Singles and Doubles Model – The Inclusion of Disconnected Triples. *J. Chem. Phys.* **1982**, *76*, 1910-1918.

[42] Scuseria, G. E.; Janssen, C. L.; Schaefer III, H. F. An Efficient Reformulation of the Closed-Shell Coupled Cluster Single and Double Excitation (CCSD) Equations. *J. Chem. Phys*. **1988**, *89*, 7382-7387.

[43] Scuseria, G. E.; Schaefer III, H. F. Is Coupled Cluster Singles and Doubles (CCSD) More Computationally Intensive Than Quadratic Configuration-Interaction (QCISD)? *J. Chem. Phys*. **1989**, *90*, 3700-3703.

[44] Yanai, T.; Tew, D. P.; Handy, N. C. A New Hybrid Exchange-Correlation Functional Using the Coulomb-Attenuating Method (Cam-B3LYP). *Chem. Phys. Lett.* **2004**, *393*, 51-57.

[45] Grimme S.; Antony J.; Ehrlich S.; Krieg H. A Consistent and Accurate Ab Initio Parameterization of Density Functional Dispersion Correction (DFT-D) for the 94 Elements H-Pu. *J. Chem. Phys.* **2010**, *132*, 154104.

[46] Grimme S.; Ehrlich S.; Goerigk L. Effect of the Damping Function in Dispersion Corrected Density Functional Theory. *J. Comp. Chem*. **2011**, *32*, 1456-1465.

[47] Dunning, T. H. Jr. Gaussian Basis Sets for Use in Correlated Molecular Calculations. I. The Atoms Boron Through Neon and Hydrogen. *J. Chem. Phys*. **1998**, *90*, 1007-1023.

[48] Kendall, R. A.; Dunning, T. H. Jr.; Harrison, R. J. Electron Affinities of the First-Row Atoms Revisited. Systematic Basis Sets and Wave Functions. *J. Chem. Phys.* **1992**, *96*, 6796-6806.

[49] Balabanov, N. B.; Peterson, K. A. Systematically Convergent Basis Sets for Transition Metals. I. All-Electron Correlation Consistent Basis Sets for the 3d Elements Sc-Zn. *J. Chem. Phys.* **2005**, *123*, 064107.

[50] Schuchardt, K. L.; Didier, B. T.; Elsethagen, T.; Sun, L.; Gurumoorthi, V.; Chase, J.; Li, J.; Windus, T. L. Basis Set Exchange: A Community Database for Computational Sciences. J. Chem. Inf. Model. **2007**, *47*, 1045-1052.

[51] Boys, S. F.; Bernardi, F. The Calculation of Small Molecular Interactions by the Differences of Separate Total Energies. Some Procedures with Reduced Errors. *Mol. Phys.* **1970**, *19*, 553-566

[52] Ohashi, K.; Sasaki J.; Yamamoto, G.; Judai, K.; Nishi, N.; Sekiya, H. Temperature Effects on Prevalent Structures of Hydrated Fe^+ Complexes: Infrared Spectroscopy and DFT Calculations of $Fe^+(H_2O)_n$ (n=3-8). *J. Chem. Phys.* **2014**, *141*, 214307.

[53] Moore, C. E. *Atomic Energy Levels;* U.S. National Bureau of Standards, Volume II, Washington D.C., 1971.

[54] Irigoras, A.; Fowler, J. E.; Ugalde, J. M. Reactivity of Cr^+ (^6S, ^4D), Mn^+ (^7S, ^5S), and Fe^+ (^6D, ^4F): Reaction of Cr^+, Mn^+, and Fe^+ with Water. *J. Am. Chem. Soc*. **1999**, *121*, 8549-8558.

[55] Glukhovtsev, M. N.; Bach, R. D.; Nagel, C. J. Performance of the B3LYP/ECP DFT Calculations of Iron-Containing Compounds. *J. Phys. Chem. A* **1997**, *101*, 316-323.

[56] Ricca, A.; Bauschlicher, C. W. A Comparison of Density Functional Theory with Ab Initio Approaches for Systems Involving First Transition Row Metals. *Theor. Chim. Acta* **1995**, *92*, 123-131.

[57] Chiodo, S.; Kondakova, O.; del Carmen Michelini, M.; Russo, N.; Sicilia, E.; Irigoras, A.; Ugalde, J. M. Theoretical Study of Two-State Reactivity of Transition Metal Cations: The "Difficult" Case of Iron Ion Interacting with Water, Ammonia, and Methane. *J. Phys. Chem. A* **2004**, *108*, 1069-1081.

[58] Chiodo S.; Russo N.; Sicilia E. Newly Developed Basis Sets for Density Functional Calculations. *J. Comput. Chem.* **2005**, *26*, 175-184.

[59] Altun, A.; Breidung, J.; Neese, F.; Thiel, W. Correlated Ab Initio and Density Functional Studies on H_2 Activation by FeO^+. *J. Chem. Theory Comput*. **2014**, *10*, 3807-3820.

[60] Garza-Galindo, R.; Castro, M.; Duncan, M. A. Theoretical Study of Nascent Hydration in the $Fe^+(H_2O)_n$ System. *J. Phys. Chem. A* **2012**, *116*, 1906-1913.

[61] Rosi, M. and Bauschlicher Jr., C. W. The Binding Energies of One and Two Water Molecules to the First Transition-Row Metal Positive Ions. *J. Chem. Phys.* **1989**, *90*, 7264-7272.

[62] Ricca, A.; Bauschlicher Jr., C. W. Successive H_2O Binding Energies for $Fe(H_2O)_n^+$. *J. Phys. Chem.* **1995**, *99*, 9003-9007.

[63] Rosenstock, H. M.; Stockbauer, R., Parr, A. C. Photoelectron–Photoion Coincidence Study of the Bromobenzene Ion. *J. Chem. Phys.* **1980**, *73*, 773-777.

[64] Malinovich, Y., Lifshitz, C. Time-Dependent Mass Spectra and Breakdown Graphs. 8. Dissociative Photoionization of Phenol. *J. Phys. Chem.* **1986**, *90*, 4311-4317.

[65] Ziesel J. P.; Lifshitz, C. Time-Dependent Mass Spectra and Breakdown Graphs. 10. Dissociative Photoionization of Anisole. *Chem. Phys.* **1987**, *117*, 227-235.

[66] Pilling, M. J.; Seakins, P. W. *Reaction Kinetics*; Oxford University Press Inc., New York, 2001.

[67] Murad, E. Thermochemical Properties of Gaseous FeO and FeOH. *J. Chem. Phys.* **1980**, *73*, 1381-1385.

[68] Cassady, C. J.; Freiser, B. S. Determination of the Iron(1+) Ion-Hydroxyl and Cobalt(1+) Ion-Hydroxyl Bond Energies by Deprotonation Reactions and by Photodissociation. *J. Am. Chem. Soc*. **1984**, *106*, 6176-6179.

[69] Magnera, T. F.; David, D. E.; Michl, J. Gas-phase Water and Hydroxyl Binding Energies for Monopositive First-row Transition-metal Ions. *J. Am. Chem. Soc.* **1989**, *111*, 4100-4101.

[70] Clemmer, D. E.; Chen, Y.-M.; Khan, F. A.; Armentrout P. B. State-Specific Reactions of $Fe^+(a^6D,a^4F)$ with D_2O and Reactions of FeO^+ with D_2. *J. Phys. Chem.* **1994**, *98*, 6522-6529.

[71] Metz, R. B.; Nicolas, C.; Ahmed, M.; Leone, S. R. Direct Determination of the Ionization Energies of FeO and CuO with VUV Radiation. *J. Chem. Phys.* **2005**, *123*, 114313.

Table 1. Theoretically Calculated Relative Energies ΔH_0 (Gibbs Energies ΔG_{298}) of $FeOH^+(H_2O)_n$ (n = 1 – 4) Isomers (kJ/mol).[a]

n		Without GD3BJ					With GD3BJ		
	complex	B3LYP[b]	B3P86[b]	MP2(full)[b]	cam-B3LYP[c]	CCSD(T)[b]	B3LYP[b]	cam-B3LYP[c]	MP2(full)[d]
1	(1,0)	**0.0 (0.0)**	**0.0 (0.0)**	**0.0 (0.0)**	**0.0 (0.0)**	**0.0 (0.0)**			
	(0,1)_A_{OH}	133.2 (131.4)	133.7 (132.0)	148.6 (146.8)	146.2 (143.5)	144.2 (142.5)			
2	(2,0)	**0.0 (0.0)**	**0.0 (0.0)**	**0.0 (0.0)**	**0.0 (0.0)**	**0.0 (0.0)**			
	(1,1)_A	27.2 (26.9)	27.1 (26.8)	37.6 (37.2)	25.0(25.9)	38.4 (38.1)			
	(1,1)_A_{OHs}	64.7 (60.8)	65.9 (61.9)	82.6 (78.7)	67.6 (64.7)	78.6 (74.7)			
	(1,1)_A_{OHe}	64.7 (61.4)	65.7 (62.4)	82.4 (79.1)	67.8 (65.7)	166.3 (163.0)			
3	(3,0)	**0.0 (0.0)**	**0.0 (0.0)**	**0.0 (0.0)**	**0.0 (0.0)**	**0.0 (0.0)**			
	(2,1)_AA	14.8 (17.7)	16.7 (19.6)	24.3 (27.2)	15.6 (17.2)	23.9 (26.8)			
	(2,1)_A	14.8 (10.4)	15.6 (11.2)	28.2 (23.8)	17.8 (11.6)	29.5 (25.1)			
	(2,1)_A_{OH}	49.1 (42.4)	51.1 (44.4)	67.6 (60.9)	57.0 (48.3)	65.8 (59.1)			
4	(3,1)_AAD_{OH}	**0.0** (8.0)	**0.0** (4.8)	**0.0** (5.0)	**0.0** (2.4)	**0.1** (6.9)	**0.0** (2.9)	**0.0** (0.9)	**0.0** (4.7)
	(3,1)_AD_{OH}	0.8 (2.9)	1.9 (0.7)	6.3 (5.5)	3.3 **(0.0)**	7.0 (8.0)	4.3 (1.1)	4.8 (**0.0**)	6.2 (5.8)
	(3,1)_AA	4.1 (1.3)	8.6 (2.6)	14.0 (8.3)	9.2 (0.9)	12.4 (8.5)	9.6 (**0.0**)	11.5 (1.2)	16.6 (10.0)
	(3,1)_A	3.5 **(0.0)**	6.8 **(0.0)**	13.3 (6.8)	9.3 (0.8)	13.2 (8.5)	11.0 (2.5)	12.6 (2.6)	15.5 (8.2)
	(4,0)_$D_{OH,a}$	6.3 (6.0)	8.5 (5.0)	3.2 **(0.0)**	7.6 (1.5)	2.4 **(1.0)**	8.0 (2.6)	8.2 (0.5)	5.3 (**0.0**)
	(4,0)_$D_{OH,b}$	6.2 (7.4)	8.4 (6.4)	3.1 (1.3)	8.5 (5.1)	**0.0 (0.0)**	7.7 (3.3)	12.2 (4.5)	5.6 (5.3)

[a] GSs are marked in bold. ZPE corrections included. [b] Geometries and vibrational frequencies determined at the B3LYP(with and without GD3BJ)/6-311+G(d,p) level and used for single-point calculations with a 6-311+G(2d,2p) basis set at each respective level shown. [c] Geometries, frequencies, and single point energies determined using the def2-TZVP basis set. [d] Values determined at the MP2(full)/pwCVTZ//B3LYP-GD3BJ/pwCVTZ level.

Table 2. Geometrical Parameters of $FeOH^+(H_2O)_n$, n = 0 – 4, Determined at B3LYP/6-311+G(d,p) Level of Theory.

Species	r(Fe-OH)	∠FeOH	r(Fe-OH_2)	∠HO-Fe-OH_2	∠H_2O-Fe-OH_2
$FeOH^+$	1.71	152.3			
(1,0)	1.71	164.5	2.00	178.4	
(0,1)_A_{OH}	1.69	151.2	4.14	17.5	
(2,0)	1.75	143.0	2.07 (1), 2.11 (2)	148.7 (1), 116.8 (2)	94.4
(1,1)_A	1.72	158.6	1.96 (1), 3.97 (2)	177.6 (1), 146.6 (2)	
(1,1)_A_{OHs}	1.70	167.3	2.01 (1), 4.31 (2)	179.3 (1), 8.1 (2)	172.6
(1,1)_A_{OHe}	1.70	160.9	2.01 (1), 4.28 (2)	178.2 (1), 11.9 (2)	169.9
(3,0)	1.79	140.4	2.10 (1), 2.15 (2), 2.20 (3)	144.1 (1), 120.1 (2), 92.1 (3)	90.1 (1-2), 110.3 (1-3), 85.8 (2-3)
(2,1)_AA	1.76	143.5	2.06 (1), 2.08 (2), 3.87 (3)	150.1 (1), 122.2 (2), 166.8 (3)	87.7 (1-2), 43.2 (1-3), 44.5 (2-3)
(2,1)_A	1.76	141.4	2.01 (1), 2.14 (2), 4.07 (3)	155.5 (1), 108.4 (2), 123.9 (3)	96.0 (1-2), 125.9 (1-3), 32.1 (2-3)
(2,1)_A_{OH}	1.74	140.5	2.08 (1), 2.13 (2), 4.23 (3)	149.7 (1), 117.6 (2), 24.7 (3)	92.6 (1-2), 125.0 (1-3), 142.3 (2-3)
(3,1)_AAD_{OH}	1.83	134.2	2.09 (1), 2.13 (2), 2.13 (3), 3.08 (4)	150.2 (1), 102.3 (2), 102.3 (3), 61.0 (4)	99.0 (1-2/3), 148.7 (1-4), 88.0 (2-3), 60.1 (2/3-4)
(3,1)_AD_{OH}	1.83	132.3	2.05(1), 2.12 (2), 2.15(3), 3.34 (4)	104.6 (1), 131.9 (2), 113.8 (3), 55.0 (4)	105.7 (1-2), 109.8 (1-3), 49.7 (1-4), 89.6 (2-3), 141.9 (2-4), 124.0 (3-4)
(3,1)_AA	1.79	140.9	2.12 (1), 2.13 (2), 2.13 (3), 3.96 (4)	107.6 (1), 125.6 (2), 125.6 (3), 131.4 (4)	105.2 (1-2/3) 84.3 (2-3), 121.1 (1-4), 43.2 (2) (2/3-4),
(3,1)_A	1.80	138.1	2.04 (1), 2.15 (2), 2.22 (3), 4.16 (4)	146.1 (1), 116.8 (2), 86.3 (3), 115.7 (4)	92.7 (1-2), 115.3 (1-3), 30.6 (1-4), 82.9 (2-3), 121.3 (2-4), 124.8 (3-4)
(4,0)_$D_{OH,a}$	1.83	136.2	2.13 (1), 2.14 (2), 2.21 (3), 2.34 (4)	120.8 (1), 130.2 (2), 109.7 (3), 76.4 (4)	103.9 (1-2), 96.3 (1-3), 75.2 (1-4), 84.1 (2-3), 96.7 (2-4), 171.4 (3-4)
(4,0)_$D_{OH,b}$	1.83	134.9	2.11 (1), 2.18 (2), 2.23 (3), 2.30 (4)	138.2 (1), 114.9 (2), 105.4 (3), 78.9 (4)	86.9 (1-2), 113.2 (1-3), 77.7 (1-4), 81.4 (2-3), 102.5 (3-4)

Table 3. Theoretically Calculated Relative Energies ΔH_0 (Gibbs Energies ΔG_{298}) of $Fe^+(H_2O)_n$ (n = 2 – 4) Isomers (kJ/mol).[a]

n		Without GD3BJ						With GD3BJ			
	Complex	B3LYP[b]	B3P86[b]	MP2(full)[b]	CCSD(T)[b]	cam B3LYP[c]	Lit[d]	B3LYP[b]	MP2(full)[b]	CCSD(T)[b]	cam B3LYP[c]
2	(2,0)	**0.0 (0.0)**	**0.0 (0.0)**	**0.0 (0.0)**	**0.0 (0.0)**	**0.0 (0.0)**	**0**[e]				
	(1,1)_A	88.2 (88.8)	87.8 (88.3)	5.4 (6.0)	100.3 (100.9)	93.8 (92.8)	95[e]				
3	(2,1)_A	**0.0 (0.0)**	**0.0 (0.0)**	**0.0 (0.0)**	**0.0 (0.0)**	**0.0 (0.0)**	**0**	**0.0 (0.0)**	**0.0 (0.0)**	**0.0 (0.0)**	**0.0 (0.0)**
	(3,0)	5.3 (6.3)	2.3 (3.3)	19.4 (20.4)	6.4 (7.4)	6.6 (9.7)	4	0.9 (1.9)	18.1 (19.1)	5.4 (6.4)	4.0 (5.0)
4	(2,2)_2D_2A	**0.0 (0.0)**	**0.0** (1.6)	85.9 (85.6)	**0.0 (0.0)**	**0.0 (0.0)**	**0**	**0.0 (0.0)**	**0.0 (0.0)**	**0.0 (0.0)**	**0.0 (0.0)**
	(2,2)_DD_2A	3.3 (1.9)	4.3 (4.5)	88.3 (86.7)	1.7 (0.4)	11.8 (12.1)	9				
	(3,1)_D_A	4.0 (1.0)	1.4 **(0.0)**	100.9 (97.6)	3.9 (0.9)	12.5 (11.7)	10	7.5 (4.5)	21.7 (18.7)	10.7 (7.7)	11.0 (8.0)
	(3,1)_AA_C_{2v}	5.4 (11.3)	2.7 (10.2)	106.0 (111.6)	30.4 (36.3)	11.0 (18.1)	8	6.6 (12.5)	27.4 (33.3)	11.4 (17.3)	8.3 (14.2)
	(3,1)_AA_C_1	6.8 (10.9)	2.7 (8.4)	120.4 (124.2)	13.0 (17.1)	12.3 (19.6)					
	(4,0)	14.3 (14.6)	8.6 (10.5)	**0.0 (0.0)**	7.1 (7.5)	23.5 (27.0)	21	13.8 (14.1)	69.4 (69.7)	32.8 (33.1)	20.0 (20.3)
	(4,0)_planar	14.0 (17.2)	9.9 (14.8)	117.3 (120.3)	14.5 (17.8)	*f*	18				

[a] GS are marked in bold. ZPE corrections included. [b] Geometries were optimized at the B3LYP(with and without GD3BJ)/6-311+G(d,p) level and used for single-point calculations with a 6-311+G(2d,2p) basis set at each respective level shown. [c] Geometries, frequencies, and single point energies determined using the def2-TZVP basis set. [d] B3LYP results at 0 K by Ohashi et al. using a 6-311+G(2df) basis set for Fe and 6-31+G(d) basis set for O and H. Frequencies scaled by 0.978 and zero-point energy corrections included.[52] [e] B3LYP/$DZVP_{opt}$ results from Garza-Galindo et al.[60] [f] Converged to (4,0).

Table 4. Fitting Parameters of eq 5 for the Experimental Collision-induced Dissociation of $FeOH^+(H_2O)_n$ Complexes, n = 1 – 4, with Xe.

Reactant	Model[a]	Product	σ_0 (Å^2)[b]	N[b]	$E_{0,PSL}$ (eV)[b]	E_0 (eV)[c]	$\Delta S^\dagger_{1000}$ [b]
$FeOH^+(H_2O)_1$	c	$FeOH^+$	23.9 ± 4.1	0.8 ± 0.1	2.35 ± 0.07		10 ± 9
		$Fe^+(H_2O)$			4.36 ± 0.16		12 ± 9
$FeOH^+(H_2O)_2$	t	$FeOH^+(H_2O)$	62.8 ± 8.6	0.7 ± 0.1	1.37 ± 0.09	1.39 ± 0.13	28 ± 13
$FeOH^+(H_2O)_2$	s	$FeOH^+(H_2O)$	63.6 ± 8.9	0.7 ± 0.1	1.38 ± 0.06		84 ± 14
		$FeOH^+$	31.9 ± 4.8		3.78 ± 0.09		42 ± 1
$FeOH^+(H_2O)_3$	t	$FeOH^+(H_2O)_2$	61.3 ± 5.1	0.9 ± 0.1	0.94 ± 0.05	0.96 ± 0.06	37 ± 19
$FeOH^+(H_2O)_3$	s	$FeOH^+(H_2O)_2$	62.9 ± 4.6	0.9 ± 0.1	0.94 ± 0.04		37 ± 21
		$FeOH^+(H_2O)$	52.6 ± 1.6		2.33 ± 0.07		29 ± 1
$FeOH^+(H_2O)_4$[d]	T	$FeOH^+(H_2O)_3$	40.6 ± 2.2	0.9 ± 0.1	0.61 ± 0.04	0.64 ± 0.06	71 ± 35
$FeOH^+(H_2O)_4$[d]	S	$FeOH^+(H_2O)_3$	41.3 ± 3.7	0.9 ± 0.1	0.62 ± 0.05		72 ± 33
		$FeOH^+(H_2O)_2$	34.4 ± 2.3		1.70 ± 0.05		31 ± 1

[a] c = competitive model, t = single channel modeling of the total cross section, and s = sequential model. [b] Lifetime effects are included. $\Delta S^\dagger_{1000}$ given in Jmol^{-1}K^{-1}. [c] E_0 modeled without lifetime effects considered. [d] Data modeled using reactant isomers that are the GS at 298 K.

Table 5. Experimental and Theoretical 0 K Bond Dissociation Energies (kJ/mol) for Loss of H_2O from $FeOH^+(H_2O)_n$.[a]

	Experiment		Without GD3BJ					With GD3BJ		
n	Primary	Secondary	B3LYP[b]	B3P86[b]	MP2(full)[b]	CCSD(T)[b]	camB3LYP[c]	B3LYP[b]	camB3LYP[c]	MP2(full)[d]
1	226.7	231.6	191.4	195.1	193.5	190.4	210.2	197.1	213.1	202.1
	± 7.1	± 5.8	(194.3)	(198.1)	(202.9)	(200.4)	(214.2)	(200.1)	(217.1)	(207.4)
2	132.2	134.1	107.6	111.2	115.4	112.7	115.4	116.9	124.2	120.4
	± 8.7	± 6.8	(110.3)	(114.0)	(124.2)	(122.1)	(120.3)	(118.1)	(127.8)	(125.7)
3	90.7	104.2	81.0	84.6	90.6	89.9	96.2	90.1	97.5	95.1
	± 4.8	± 2.9	(84.0)	(87.7)	(101.0)	(100.5)	(101.7)	(93.1)	(103.0)	(101.6)
4[e]	58.5		56.7	59.5	63.1	64.1	72.3	68.4	80.5	47.1
	± 3.8		(60.3)	(63.2)	(75.0)	(76.8)	(77.4)	(71.3)	(85.1)	(81.0)
MAD[f]	Primary		18	15	14	16	13	14	13	13
MAD[g]		Secondary	30	26	24	26	16	22	12	17

[a] Theoretical values are given with (without) counterpoise corrections. ZPE corrections included. [b] Calculated using a 6-311+G(2d,2p) basis set and B3LYP(with or without GD3BJ)/6-311+G(d,p) geometries. [c] Calculated using a def2-TZVP basis set. [d] Values determined at the MP2(full)/pwCVTZ//B3LYP-GD3BJ/pwCVTZ level. [e] Calculated using 298 K GS from Table 1. [f] Mean absolute deviation towards primary experimental BDEs. [g] Mean absolute deviation towards secondary experimental BDEs.

Table 6. Experimental and Theoretical 0 K Bond Dissociation Energies (kJ/mol) for Loss of Water Molecules from $Fe^+(H_2O)_n$. [a]

		Without GD3BJ					With GD3BJ			
n	Exp.[b]	B3LYP[c]	B3P86[c]	MP2(full)[c]	CCSD(T)[c]	camB3LYP[d]	B3LYP[c]	MP2(full)[c]	CCSD(T)[c]	camB3LYP[c]
1[e]	128.3	132.8	136.9	122.7	125.1	145.6	139.8	123.3	125.1	148.7
	± 4.8	(135.3)	(139.4)	(129.7)	(131.9)	(148.8)	(142.1)	(129.5)	(131.8)	(151.8)
2[e]	164.0	153.4	151.2	109.1	149.3	168.2	158.0	107.3	149.8	170.7
	± 3.9	(156.3)	(154.1)	(67.0)	(159.7)	(172.1)	(160.9)	(66.2)	(160.2)	(174.7)
3	76.2	64.4	67.4	61.3	60.1	74.4	68.8	60.9	64.8	76.8
	± 3.9	(66.4)	(69.5)	(67.8)	(67.1)	(76.9)	(70.9)	(67.9)	(67.4)	(79.4)
4[f]	50.2	53.4	54.6	137.0	50.4	69.7	64.7	58.0	57.0	72.2
	± 6.8	(55.4)	(56.6)	(143.3)	(57.2)	(72.2)	(66.7)	(64.4)	(63.9)	(74.8)
MAD[g]		8	9	41	9	11	10	21	9	12

[a] Theoretical values are given with (without) counterpoise correction. ZPE corrections included. [b] Experimental values taken from Dalleska et al.[8] [c] Calculated using a 6-311+G(2d,2p) basis set and B3LYP(with or without GD3BJ)/6-311+G(d,p) geometries and zero-point energy corrections. [d] Calculated using a def2-TZVP basis set. [e] For all levels of theory except CCSD(T), BDEs were computed on quartet and sextet surface and product asymptotes were adjusted to match experiment for the Fe^+ (^6D) ground state, see text. [f] Calculated using 298 K GS from Table 3. [g] Mean absolute deviation of theoretical BDEs compared to experimental results.

Table 7. Experimental and Theoretical 0 K Bond Dissociation Energies (kJ/mol) for Loss of the Hydroxide Group from $FeOH^+(H_2O)_n$ [a]

		Without GD3BJ					With GD3BJ		
n	Exp.[b]	B3LYP[c]	B3P86[c]	MP2(full)[c]	CCSD(T)[c]	camB3LYP[d]	B3LYP[c]	camB3LYP[d]	MP2(full)[c]
0[e]	322.3	322.5	335.1	279.2	317.8	324.4	326.6	326.3	280.6
	±17.6	(325.7)	(338.4)	(191.2)	(330.7)	(327.4)	(329.8)	(329.3)	(291.3)
1[e]	420.7	381.3	393.4	350.1	384.7	389.2	384.3	391.3	349.2
	±15.4	(384.8)	(397.1)	(364.5)	(399.1)	(392.7)	(387.8)	(394.8)	(363.6)
2	388.9	335.3	353.2	407.8	346.4	336.8	341.5	343.5	407.8
	±18.1	(338.8)	(356.9)	(421.7)	(361.6)	(340.9)	(345.0)	(347.6)	(421.7)
3	403.4	352.6	371.3	440.1	378.9	361.2	363.6	367.0	440.0
	±19.1	(356.2)	(375.2)	(454.8)	(395.0)	(365.7)	(367.2)	(371.5)	(454.7)
4[f]	411.7	356.8	375.7	369.3	395.7	365.1	367.5	377.0	443.7
	±20.6	(361.2)	(380.4)	(386.5)	(414.7)	(370.8)	(371.9)	(382.7)	(458.0)
MAD[g]		40	29	42	25	35	34	30	40

[a] Theoretical values are given with (without) counterpoise correction. ZPE corrections included. [b] Experimental values derived in this work. [c] Calculated using a 6-311+G(2d,2p) basis set and B3LYP(with or without GD3BJ)/6-311+G(d,p) geometries. [d] Calculated using a def2-TZVP basis set. [e] For all levels except CCSD(T), BDEs were computed on quartet and sextet surface and product asymptotes were adjusted to match experiment for the Fe^+ (^6D) ground state, see text. [f] Calculated using 298 K GS from Table 2. [g] Mean absolute deviation of theoretical BDEs compared to experimental results.

Figure Captions

Figure 1. Low-energy isomers of $FeOH^+(H_2O)_n$ with n = 0 – 4, optimized at B3LYP/6-311+G(d,p) level of theory. For n = 4, all low-lying isomeres are presented as they are very similar in energy.

Figure 2. Experimental dissociation cross sections of $FeOH^+(H_2O)_n$, n = 1 – 4 versus lab frame (upper x-axis) and center-of-mass frame (lower x-axis) collision energy are shown for a Xe collison gas pressure of 0.2 mTorr. The sum of the primary and secondary product cross sections represents the total cross section (black line).

Figure 3. Zero-pressure extrapolated cross sections for the dissociation of $FeOH^+(H_2O)_n$ complexes with Xe as a function of lab-frame (upper x-axis) and center-of-mass frame (lower x-axis) collision energies. Models of eq 5 are represented by solid lines and dashed lines represent the models in the absence of internal and kinetic energy distributions. Sequential dissociation models are utilized for n = 2 – 4 whereas a competitive model is applied for n = 1.

Figure 4. Experimental BDEs given in kJ/mol presented in this work (blue arrows) together with published results by Dalleska et al.[8] (red arrows) and derived BDEs for the loss of the hydroxide group (green arrows).

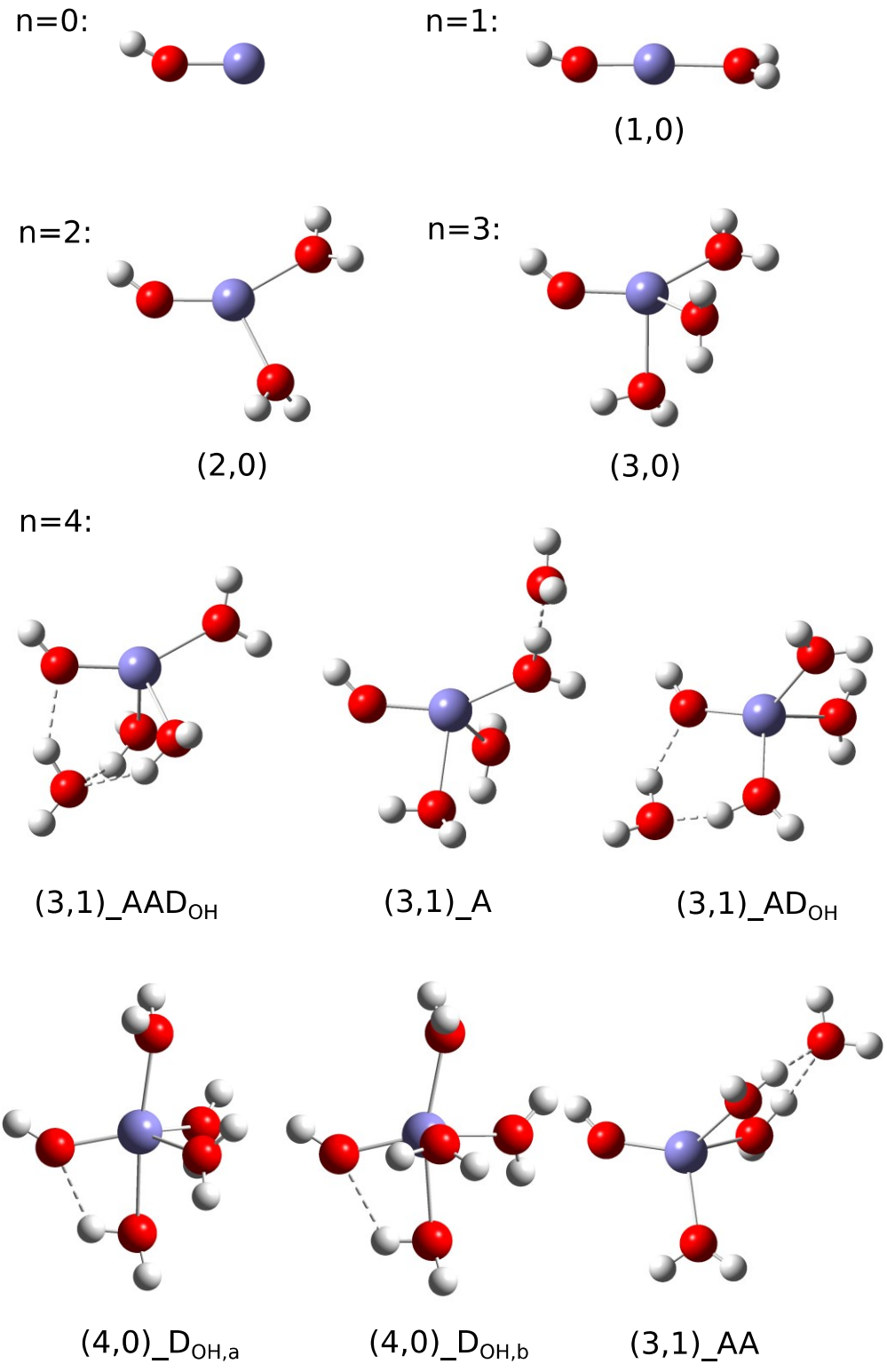

Figure 1

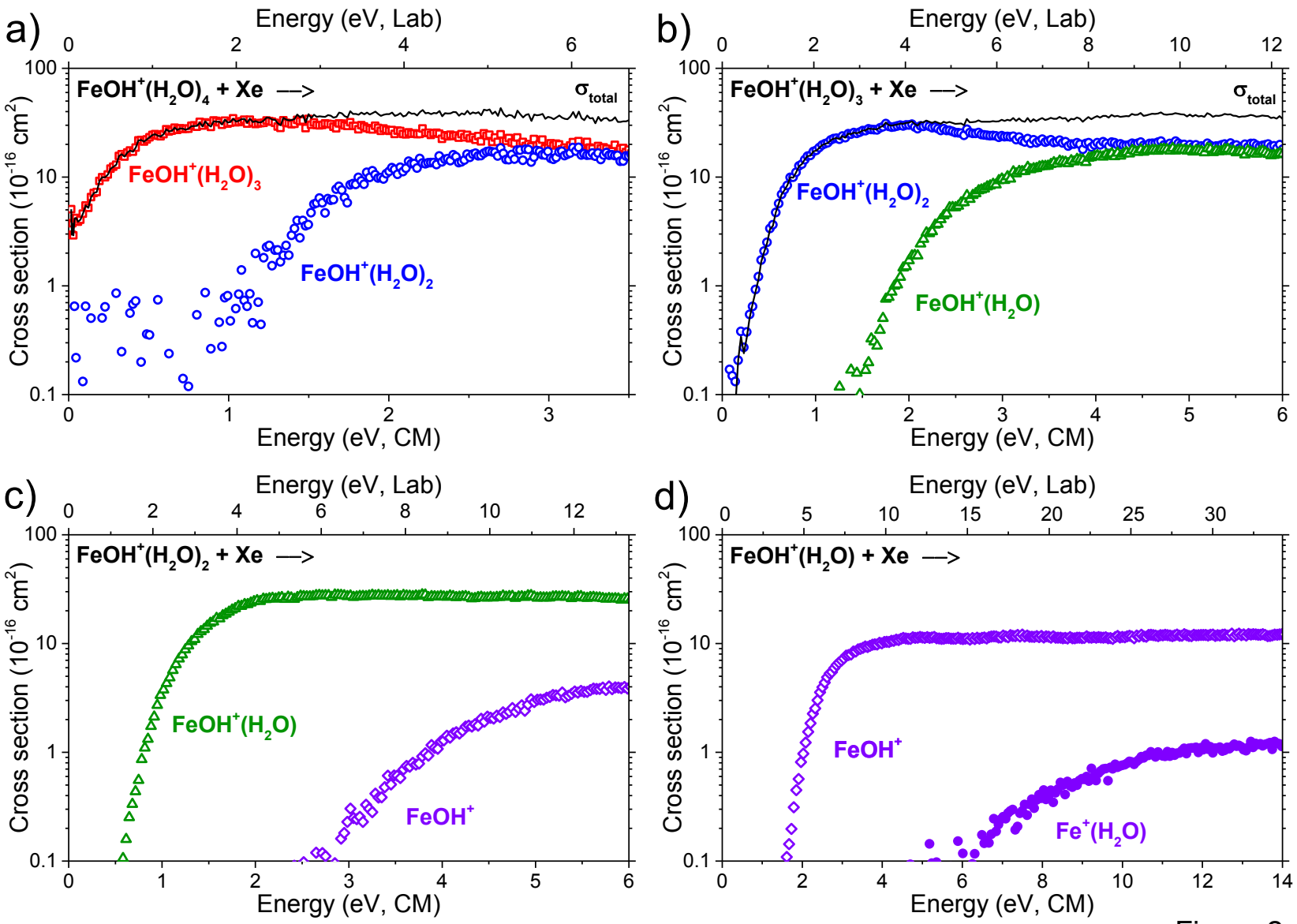
a)
Energy (eV, Lab)
FeOH+(H2O)4 + Xe —>
σtotal
FeOH+(H2O)3
FeOH+(H2O)2
Cross section (10-16 cm2)
Energy (eV, CM)
b)
Energy (eV, Lab)
FeOH+(H2O)3 + Xe —>
σtotal
FeOH+(H2O)2
FeOH+(H2O)
Cross section (10-16 cm2)
Energy (eV, CM)
c)
Energy (eV, Lab)
FeOH+(H2O)2 + Xe —>
FeOH+(H2O)
FeOH+
Cross section (10-16 cm2)
Energy (eV, CM)
d)
Energy (eV, Lab)
FeOH+(H2O) + Xe —>
FeOH+
Fe+(H2O)
Cross section (10-16 cm2)
Energy (eV, CM)

Figure 2

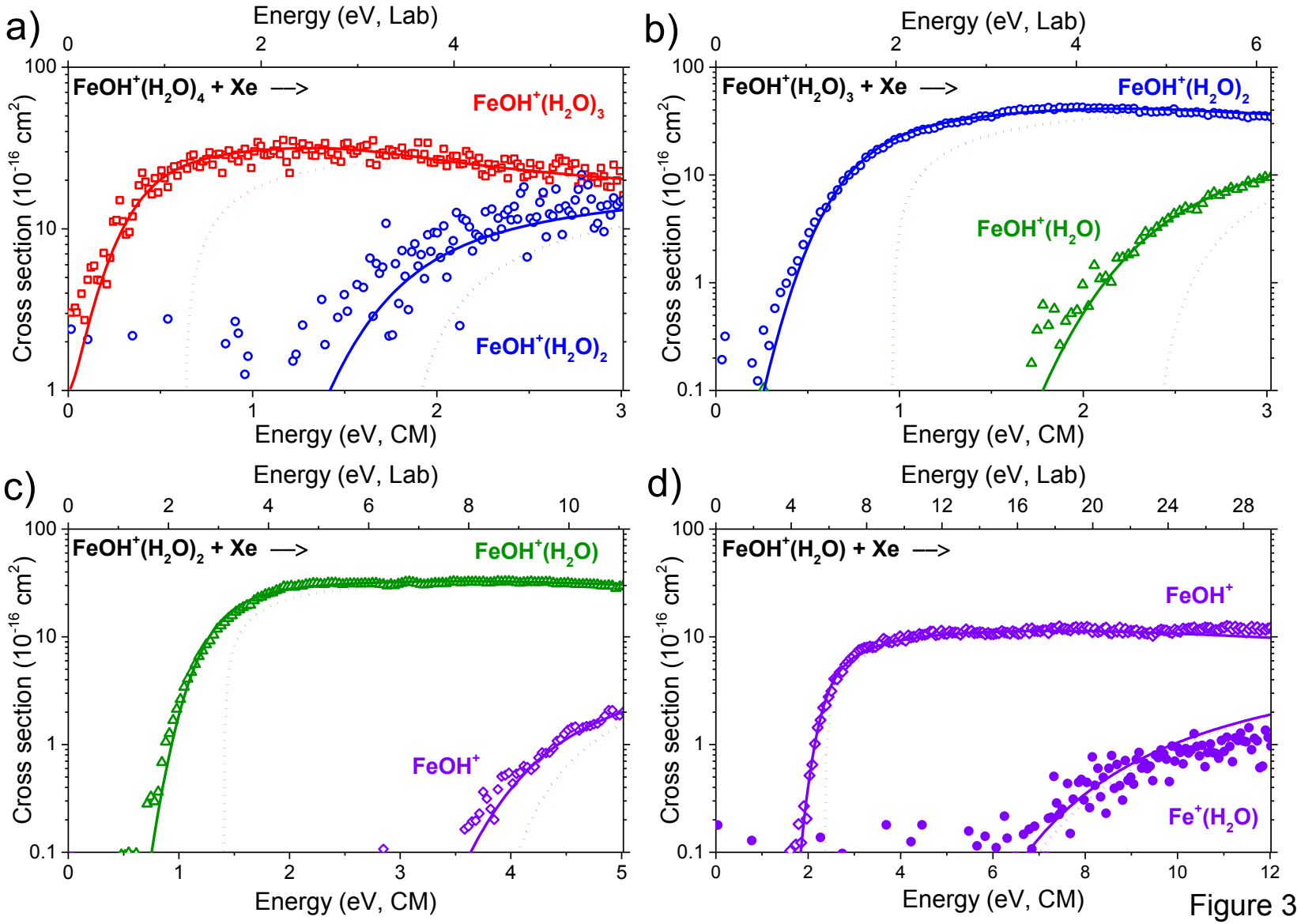
a)
Energy (eV, Lab)
FeOH+(H2O)4 + Xe —>
FeOH+(H2O)3
FeOH+(H2O)2
Cross section (10-16 cm2)
Energy (eV, CM)
b)
Energy (eV, Lab)
FeOH+(H2O)3 + Xe —>
FeOH+(H2O)2
FeOH+(H2O)
Cross section (10-16 cm2)
Energy (eV, CM)
c)
Energy (eV, Lab)
FeOH+(H2O)2 + Xe —>
FeOH+(H2O)
FeOH+
Cross section (10-16 cm2)
Energy (eV, CM)
d)
Energy (eV, Lab)
FeOH+(H2O) + Xe —>
FeOH+
Fe+(H2O)
Cross section (10-16 cm2)
Energy (eV, CM)

Figure 3

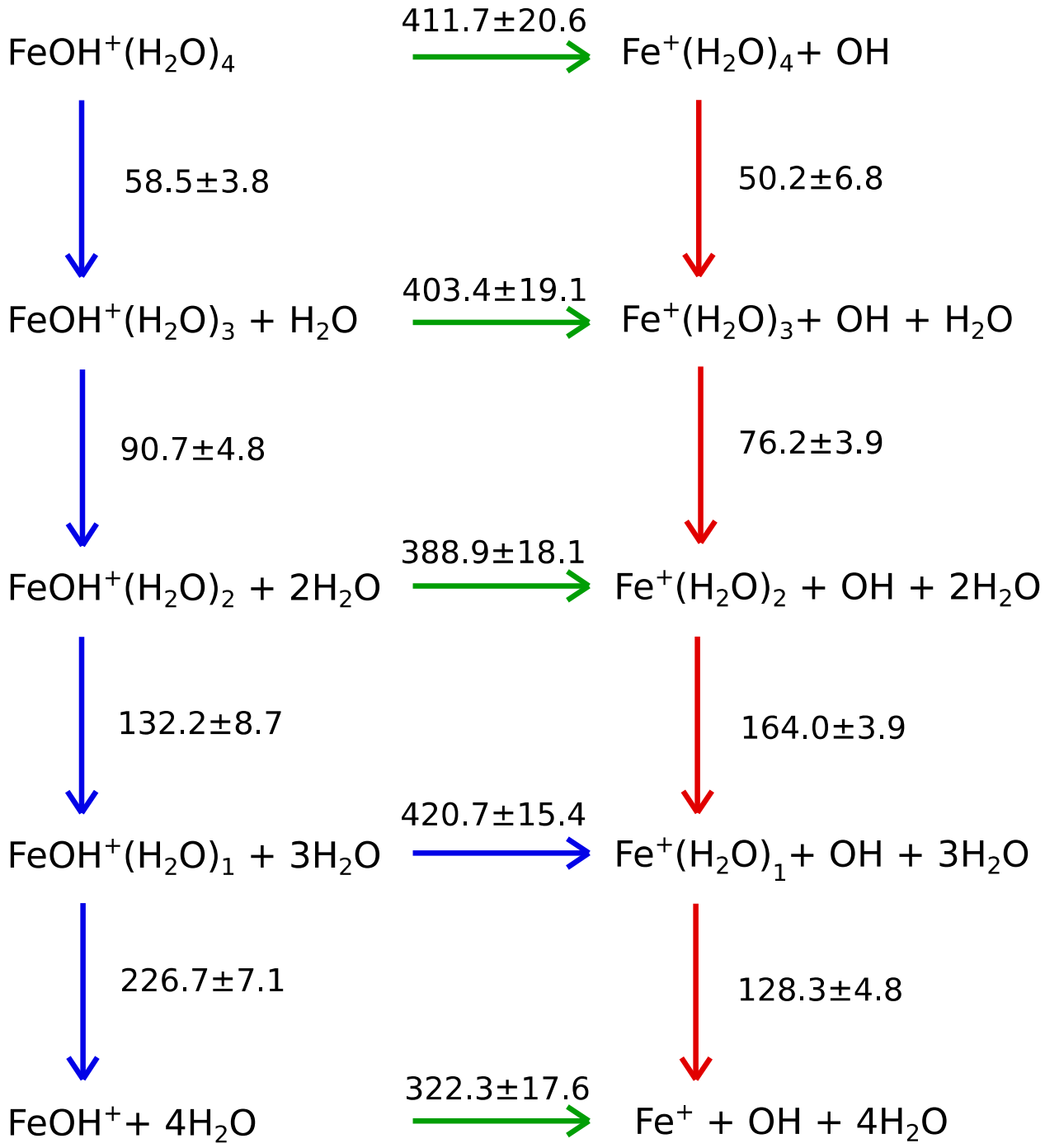
FeOH+(H2O)4
411.7±20.6
Fe+(H2O)4+ OH
58.5±3.8
50.2±6.8
FeOH+(H2O)3 + H2O
403.4±19.1
Fe+(H2O)3+ OH + H2O
90.7±4.8
76.2±3.9
FeOH+(H2O)2 + 2H2O
388.9±18.1
Fe+(H2O)2 + OH + 2H2O
132.2±8.7
164.0±3.9
FeOH+(H2O)1 + 3H2O
420.7±15.4
Fe+(H2O)1+ OH + 3H2O
226.7±7.1
128.3±4.8
FeOH+ + 4H2O
322.3±17.6
Fe+ + OH + 4H2O

Figure 4

TOC Graphic

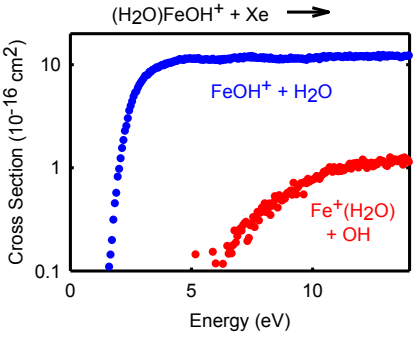
(H2O)FeOH+ + Xe
Cross Section (10-16 cm2)
10
1
0.1
0
5
10
Energy (eV)
FeOH+ + H2O
Fe+(H2O)
+ OH

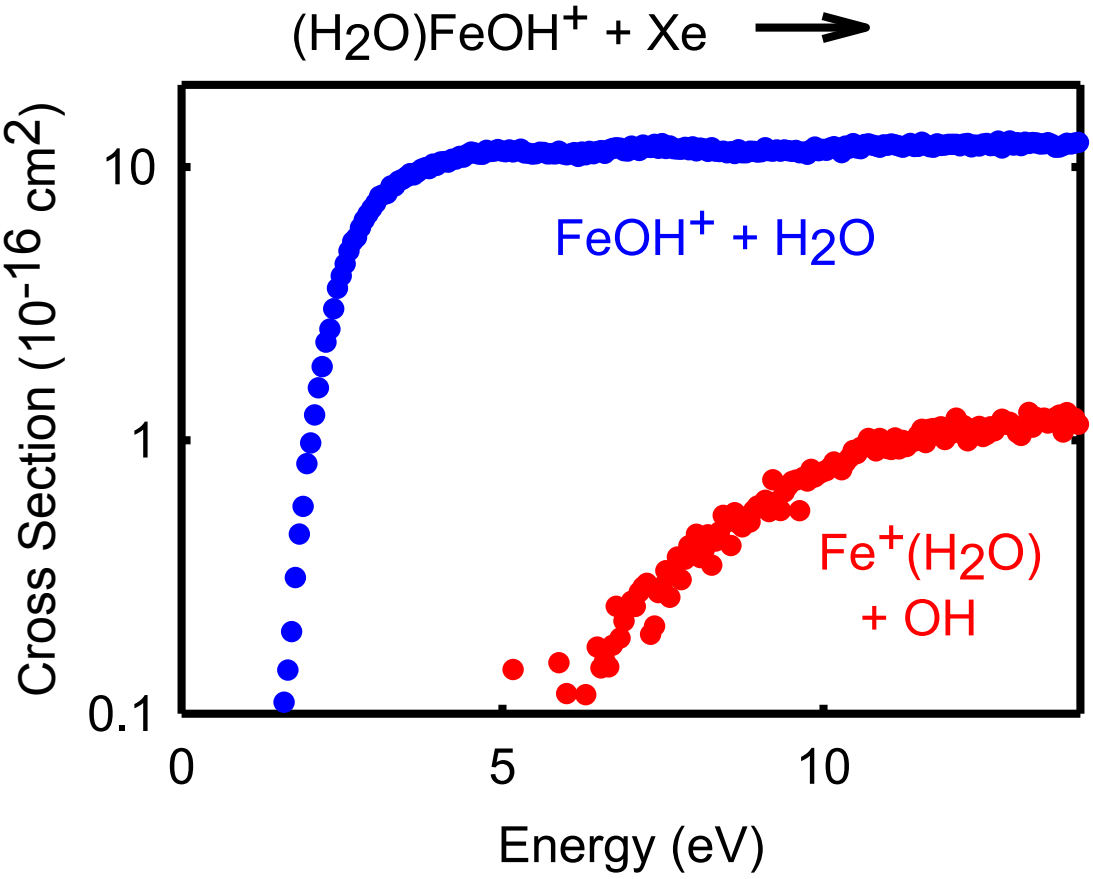
(H2O)FeOH+ + Xe
Cross Section (10-16 cm2)
10
1
0.1
0
5
10
Energy (eV)
FeOH+ + H2O
Fe+(H2O)
+ OH